Beam wakes for canonical chambers with anisotropic surface impedance

Igor Zagorodnov and Martin Dohlus
Deutsches Elektronen-Synchrotron DESY, Notkestrasse 85, 22607 Hamburg, Germany

(Received 10 July 2023; accepted 23 August 2023; published 6 September 2023)

We consider analytical expressions for beam impedance of round, rectangular, and Π-shaped waveguides with anisotropic surface impedance of arbitrary nature. The formulas are given for relativistic and nonrelativistic cases and the impedance matrix of general form. The field matching technique for layered structures with layers of uniaxial anisotropy and anisotropic impedance boundary condition at the last layer is described. The analytical methods are applied to the real structure examples with corrugations, dielectrics, and anomalous skin effects.

DOI: 10.1103/PhysRevAccelBeams.26.094401

I. INTRODUCTION

The electromagnetic behavior of the vacuum chamber in many situations can be described by impedance boundary condition for time-harmonic electromagnetic field $\boldsymbol{E}$, $\boldsymbol{H}$ [1,2]:

$$\boldsymbol{n} \times \boldsymbol{E} = -\boldsymbol{Z}^s[\boldsymbol{n} \times (\boldsymbol{n} \times \boldsymbol{H})], \tag{1}$$

where $\boldsymbol{Z}^s$ is a surface impedance tensor and $\boldsymbol{n}$ is a unit vector normal to the surface of the pipe.

The explicit form of the surface impedance tensor depends on the material and geometry properties of the pipe. The resistivity and the roughness are analyzed in [2–4]. The structures with periodic corrugations of the walls are considered in [5–8]. The anomalous skin effects can be treated as in [9,10].

In this paper we consider analytical expressions for beam impedance [11] of round, rectangular and Π-shaped waveguides with anisotropic surface impedance of arbitrary nature.

Equations for round structure with impedance boundary condition for nonrelativistic charge have been revisited recently in [3] for monopole and dipole modes. In the relativistic limit the equations for dipole mode are written only for the explicit form of the resistive surface impedance without generalization to an arbitrary one. The equations for higher order azimuthal modes are not considered there. The knowledge of the higher order modes is necessary to analyze the beam behavior near to the walls of the vacuum chamber. The application of the surface impedance formalism to flat corrugated structures with one or two parallel plates was done in [6–8]. But only the relativistic limit was studied in these papers.

In the publications listed above the surfaces impedance matrix has only diagonal elements, which are equal. But, for example, in the case of the corrugated structures with resistivity a more accurate approximation is to use nonequal diagonal elements, as it was done for the longitudinal impedance in [12]. The impedance matrix with nonequal diagonal elements was used in [13,14] for the analysis of radiation from the charged particle near a corrugated surface.

Examples of surfaces characterized by fully populated impedance matrices are discussed in Refs. [15,16]. The accuracy of the surface impedance boundary conditions for dielectric layers and conductive metals have been examined, for example, in [16,17], along with references therein.

Round layered pipes and flat layered parallel plates are considered in [18] for fully isotropic layers and in [19] for anisotropic materials. The treatment of the impedance boundary condition in the last layer was not considered there.

In this paper we would like to extend the available results in several directions. We consider all modes for round, rectangular, and Π-shaped structures in nonrelativistic and relativistic cases. We give the equations for impedance matrix of general form.

In the following we call the structure "round" if it is axially symmetric. If the structure has a constant width between two perfectly conducting planes and has rectangular cross sections then we call such structure "rectangular." Figure 1 shows the transverse to z-axis cross sections of round and rectangular structures. Additionally, a Π-shaped structure is shown in Fig. 1 as well. It is one plate between two perfectly conducting plates.

We assume that the charge is moving along a straight line parallel to the longitudinal axis of the system, and we neglect the influence of the wakefields on the charge motion. In the frequency domain all fields will have the

Published by the American Physical Society under the terms of the Creative Commons Attribution 4.0 International license. Further distribution of this work must maintain attribution to the author(s) and the published article's title, journal citation, and DOI.

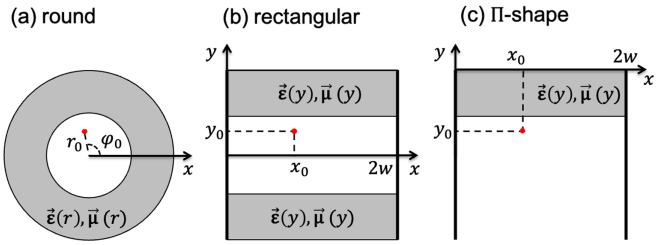

FIG. 1. Transverse to z-axis cross sections of round (a), rectangular (b), and Π-shaped (c) geometries. The point charge position is shown by red circle.

time dependence $e^{i\omega t}$ (ω is the angular frequency) which we will omit in the subsequent equations.

We start in Sec. II A with derivation of the nonrelativistic beam impedance of round metallic pipe with anisotropic surface impedance. Then the equations for the relativistic limit are presented. The same is done in Secs. II B and II C for the rectangular pipe and Π-shape. In Sec. II D we present the equations for the infinite and semi-infinite flat plates. Section III describes the field matching technique for layered structures with uniaxial anisotropy and anisotropic impedance boundary condition. The analytical techniques and numerical methods are applied to the real structure examples with corrugations, dielectrics and anomalous skin effects in Sec. IV.

II. VACUUM REGION CLOSED BY PIPE WITH SURFACE IMPEDANCE

Let us start by considering only one vacuum region closed with a metallic pipe. In this case we will derive analytical solutions. In Sec. III we discuss how to modify the field matching method for the pipes with many homogeneous layers.

A. Round beam pipe with surface impedance

For round structures we will use cylindrical coordinates r, φ, z. The charge density in the frequency domain can be expanded in Fourier series

$$\rho(r,\varphi,z,k) = e^{-ikz/\beta}\sum_{m=0}^{\infty}\rho_m\delta(r-r_0)\cos[m(\varphi-\varphi_0)],$$
$$\rho_m = \frac{q}{\pi v r_0(1+\delta_{m0})}, \tag{2}$$

where r_0, φ_0 are coordinates of the point charge q, $k = \omega/c$, $\beta = v/c$, c is velocity of light in vacuum, and $\delta_{m0} = 1$ if $m = 1$, 0 otherwise.

From the linearity of Maxwell's equations the components of the electromagnetic field can be represented by infinite sums:

$$\begin{pmatrix} H_\varphi(r,\varphi,z,k) \\ E_r(r,\varphi,z,k) \\ E_z(r,\varphi,z,k) \end{pmatrix} = e^{-ikz/\beta}\sum_{m=0}^{\infty}\begin{pmatrix} H_{\varphi m}(r,k) \\ E_{rm}(r,k) \\ E_{zm}(r,k) \end{pmatrix}\cos(m\varphi),$$
$$\begin{pmatrix} E_\varphi(r,\varphi,z,k) \\ H_r(r,\varphi,z,k) \\ H_z(r,\varphi,z,k) \end{pmatrix} = e^{-ikz/\beta}\sum_{m=0}^{\infty}\begin{pmatrix} E_{\varphi m}(r,k) \\ H_{rm}(r,k) \\ H_{zm}(r,k) \end{pmatrix}\sin(m\varphi). \tag{3}$$

It is a direct consequence of Maxwell's equations applied to fields' decomposition in Eq. (3), that for each modal number m we can write an independent system of equations

$$\begin{aligned}
\frac{m}{r}H_{zm} + i\frac{k}{\beta}H_{\varphi m} &= i\omega\epsilon_0 E_{rm},\\
-i\frac{k}{\beta}H_{rm} - \frac{\partial}{\partial r}H_{z,m} &= i\omega\epsilon_0 E_{\varphi m},\\
\frac{1}{r}\frac{\partial}{\partial r}(rH_{\varphi m}) - \frac{m}{r}H_{rm} &= i\omega\epsilon_0 E_{zm} + v\rho_m\delta(r-r_0),\\
-\frac{m}{r}E_{zm} + i\frac{k}{\beta}E_{\varphi m} &= -i\omega\mu_0 H_{r,m},\\
-i\frac{k}{\beta}E_{rm} - \frac{\partial}{\partial r}E_{z,m} &= -i\omega\mu_0 H_{\varphi m},\\
\frac{1}{r}\frac{\partial}{\partial r}(rE_{\varphi m}) + \frac{m}{r}E_{r,m} &= -i\omega\mu_0 H_{zm},\\
\frac{1}{r}\frac{\partial}{\partial r}(rH_{rm}) - \frac{m}{r}H_{\varphi,m} - ikH_{zm} &= 0,\\
\frac{1}{r}\frac{\partial}{\partial r}(rE_{rm}) + \frac{m}{r}E_{\varphi m} - ikE_{zm} &= \frac{\rho_m}{\epsilon_0}.
\end{aligned} \tag{4}$$

The impedance boundary condition, Eq. (1), can be rewritten as

$$\begin{pmatrix} -E_{zm}(a) \\ E_{\varphi m}(a) \end{pmatrix} = \begin{pmatrix} Z_{TM} & Z_{12} \\ Z_{21} & Z_{TE} \end{pmatrix}\begin{pmatrix} H_{\varphi m}(a) \\ H_{zm}(a) \end{pmatrix}. \tag{5}$$

We are interested in beam impedance as defined in [11,18].

$$Z_\parallel(r_0,\varphi_0,r,\varphi,k,\gamma) = \frac{E_z(r,\varphi,z,k)e^{ikz/\beta}}{q}, \tag{6}$$

where the longitudinal field E_z depends on the coordinates of the source particle r_0, φ_0 and the product $E_z e^{ikz/\beta}$ is independent of z. For round pipe the beam impedance can be presented as expansion in azimuthal modes

$$Z_{\parallel}(r_0,\varphi_0,r,\varphi,k,\gamma)=\sum_{m=0}^{\infty}Z_m(k,\gamma)I_m\left(\frac{kr_0}{\gamma\beta}\right)I_m\left(\frac{kr}{\gamma\beta}\right)\cos[m(\varphi-\varphi_0)]+Z_{sc}^{\infty}(r_0,\varphi_0,r,\varphi,k,\gamma), \tag{7}$$

$$Z_{sc}^{\infty}(r_0,\varphi_0,r,\varphi,k,\gamma)=-\frac{kZ_0}{2\pi(\gamma^2-1)}K_0\left(\frac{k\sqrt{r_0^2+r^2-2r_0r\cos(\varphi-\varphi_0)}}{\gamma\beta}\right), \tag{8}$$

where I_m, K_0 are modified Bessel functions of complex argument, γ is the Lorentz factor and we have written explicitly the space charge contribution Z_{sc}^{∞}. Function $Z_m(k,\gamma)$ is the modal impedance to be found.

From system of first-order equations, Eq. (4), we obtain the decoupled second-order equations for the longitudinal field components

$$\frac{1}{r}\frac{\partial}{\partial r}r\frac{\partial}{\partial r}E_{zm}-\left(\frac{m^2}{r^2}+\nu^2\right)E_{zm}=\frac{ik}{\gamma^2\beta\epsilon_0}\rho_m\delta(r-r_0), \tag{9}$$

$$\frac{1}{r}\frac{\partial}{\partial r}r\frac{\partial}{\partial r}H_{zm}-\left(\frac{m^2}{r^2}+\nu^2\right)H_{zm}=0,\qquad \nu=\frac{k}{\gamma\beta}. \tag{10}$$

A general solution of homogeneous hyperbolic Eqs. (9) and (10) in charge free regions can be written in form

$$\begin{aligned}E_{zm}(r)&=C_I^mI_m(\nu r)+C_K^mK_m(\nu r),\\ H_{zm}(r)&=D_I^mI_m(\nu r)+D_K^mK_m(\nu r),\end{aligned} \tag{11}$$

where I_m, K_m are modified Bessel functions of complex argument and C_I^m, C_K^m, D_I^m, D_K^m are unknown constants to be found.

In the following we numerate the electric field $E_{zm}(r)$ by index "0" for $r<r_0$ and by index "1" for $r>r_0$. The magnetic field $H_{zm}(r)$ has the same representation in the whole domain. In order to avoid the divergence of the solution we need to put $C_K^{m,0}=0$, $D_K^m=0$. At the position of the beam r_0 the longitudinal component of the electric field E_z is continuous and we can write

$$C_I^{m,0}=C_I^{m1}+C_K^{m,1}\frac{K_m(\nu r)}{I_m(\nu r)}. \tag{12}$$

If we multiply Eq. (9) by r, integrate it from $r_0-\Delta$ to $r_0-\Delta$ and take limit for $\Delta\to 0$ then we obtain the jump condition of the derivative:

$$\frac{\partial}{\partial r}E_{zm}^1(r_0)-\frac{\partial}{\partial r}E_{zm}^0(r_0)=\frac{ik}{\gamma^2\beta\epsilon_0}\rho_m. \tag{13}$$

It follows from Eqs. (11) and (13) that

$$\begin{aligned}&C_I^{m,1}\frac{d}{dr}I_m(\nu r_0)+C_K^{m,1}\frac{d}{dr}K_m(\nu r_0)-C_I^{m,0}\frac{d}{dr}I_m(\nu r_0)\\&\quad=\frac{ik}{\gamma^2\beta\epsilon_0}\rho_m.\end{aligned} \tag{14}$$

As a next step we put Eq. (12) into Eq. (14) and use the relation $I_m(x)\frac{d}{dx}K_m(x)-K_m(x)\frac{d}{dx}I_m(x)=-\frac{1}{x}$. We obtain

$$C_K^{m,1}=-\frac{ikr_0}{\gamma^2\beta\epsilon_0}\rho_mI_m(\nu r_0). \tag{15}$$

It is direct consequence of Eq. (7) that the impedance term can be found as

$$Z_m(k,\gamma)=\frac{E_{zm}^1(r_0)-qZ_{sc,m}^m}{qI_m(\nu r_0)^2}=\frac{C_I^{m,1}}{qI_m(\nu r_0)}, \tag{16}$$

where we have used the expansion of the space charge impedance in azimuthal modes

$$\begin{aligned}&Z_{sc}(r_0,\varphi_0,r,\varphi,k,\gamma)\\&\quad=\sum_{m=0}^{\infty}Z_{sc,m}(r_0,r,k,\gamma)\cos[m(\varphi-\varphi_0)],\end{aligned} \tag{17}$$

$$\begin{aligned}Z_{sc,m}(r_0,r,k,\gamma)&=\frac{ikZ_0}{\pi(\gamma^2-1)(1+\delta_{m0})}K_m(\nu r)I_m(\nu r_0)\\&=\frac{C_K^{m,1}}{q}K_m(\nu r),\qquad r\ge r_0.\end{aligned} \tag{18}$$

In order to find the constants C_I^{m1}, D_I^m in Eq. (11) we use the impedance boundary condition, Eq. (5), with the azimuthal field components defined through the longitudinal ones as

$$H_{\varphi m}^1=\frac{ik}{\nu^2}\left(\frac{1}{Z_0}\frac{\partial}{\partial r}E_{zm}^1+\frac{m}{\beta r}H_{zm}\right), \tag{19}$$

$$E_{\varphi m}^1=-\frac{ik}{\nu^2}\left(Z_0\frac{\partial}{\partial r}H_{zm}+\frac{m}{\beta r}E_{zm}^1\right). \tag{20}$$

From straightforward symbolic calculations [20] we derive that the modal impedance in Eq. (7) can be written as

$$\begin{aligned}Z_m(k,\gamma)&=\frac{\theta Z_{\mathrm{TM}}N}{\pi aI_m(x)(1+\delta_{m0})D}+Z_{\mathrm{pipe},m}(k,\gamma),\\ \theta&=\frac{x}{ak},\qquad x=\frac{ka}{\gamma\beta},\end{aligned} \tag{21}$$

$$N=I_m(x)\left(\frac{\theta|\boldsymbol{Z}^s|}{Z_0Z_{\mathrm{TM}}}-\frac{im}{x}\right)+iI_{m-1}(x), \tag{22}$$

$$D = I_m(x)^2\left(\frac{(1-\beta^2)m^2 Z_{\mathrm{TM}}}{\beta^2 x^2 Z_0} - \frac{i\theta m}{x}\left(1+\frac{|\boldsymbol{Z}^s|}{Z_0^2}+\frac{Z_{12}-Z_{21}}{\beta Z_0}\right)+\frac{\theta^2 Z_{\mathrm{TE}}}{Z_0}\right) + I_m(x)I_{m-1}(x)\left(\frac{2mZ_{\mathrm{TM}}}{xZ_0}+i\theta\left(1+\frac{|\boldsymbol{Z}^s|}{Z_0^2}\right)\right) - I_{m-1}(x)^2\frac{Z_{\mathrm{TM}}}{Z_0}, \tag{23}$$

$$Z_{\mathrm{pipe},m}(k,\gamma) = \frac{ix^2 Z_0 K_m(x)}{a^2 k\pi I_m(x)(1+\delta_{m0})}, \tag{24}$$

where $|\boldsymbol{Z}^s|$ is the determinant of the matrix $\boldsymbol{Z}^s$:

$$|\boldsymbol{Z}^s| = Z_{\mathrm{TE}}Z_{\mathrm{TM}} - Z_{12}Z_{21}. \tag{25}$$

Here $Z_{\mathrm{pipe},m}(k,\gamma)$ is the modal impedance of nonrelativistic charge in perfectly conducting round pipe.

In relativistic limit, $\gamma \to \infty$, one obtains

$$Z_{\parallel}(r_0,\varphi_0,r,\varphi,k,\gamma) = \sum_{m=0}^{\infty} Z_m(k) r_0^m r^m \cos[m(\varphi-\varphi_0)], \tag{26}$$

$$Z_0(k) = \frac{Z_{\mathrm{TM}}}{2a\pi(1+\frac{iak}{2}\frac{Z_{\mathrm{TM}}}{Z_0})}, \tag{27}$$

$$Z_m(k) = \frac{Z_{\mathrm{TM}}}{a^{2m+1}\pi(1+\frac{Z_{21}-Z_{12}}{Z_0}+\frac{|\boldsymbol{Z}^s|}{Z_0^2}+(\frac{m}{ika}+\frac{iak}{m+1})\frac{Z_{\mathrm{TM}}}{Z_0})}, \quad m>0. \tag{28}$$

B. Rectangular beam pipe with surface impedance at two opposite sidewalls

In rectangular case we choose a coordinate system with y in the vertical and x in the horizontal directions as it is shown in Fig. 1. The z coordinate is directed along the beam direction. The structures considered in this paper have constant width $2w$ in x-direction between two perfectly conducting side walls. In the following we consider only the case where the rectangular structure is symmetric in the y-direction (up-bottom symmetry).

The charge density can be expanded in Fourier series along x-coordinate

$$\rho(x,y,z,k) = \frac{e^{-ikz/\beta}}{w}\sum_{m=1}^{\infty}\rho_m\delta(y-y_0)\sin(k_{xm}x_0)\sin(k_{xm}x), \qquad \rho_m = \frac{q}{v}, \qquad k_{xm} = \frac{\pi m}{2w}, \tag{29}$$

where x_0, y_0 are coordinates of the point charge. Again it follows from the linearity of Maxwell's equations that the components of electromagnetic field can be represented by infinite sums:

$$\begin{pmatrix} H_x(x,y,z,k)\\ E_y(x,y,z,k)\\ E_z(x,y,z,k)\end{pmatrix} = \frac{e^{-ikz/\beta}}{w}\sum_{m=1}^{\infty}\begin{pmatrix} H_{xm}(y,k)\\ E_{ym}(y,k)\\ E_{zm}(y,k)\end{pmatrix}\sin(k_{xm}x),$$

$$\begin{pmatrix} E_x(x,y,z,k)\\ H_y(x,y,z,k)\\ H_z(x,y,z,k)\end{pmatrix} = \frac{e^{-ikz/\beta}}{w}\sum_{m=1}^{\infty}\begin{pmatrix} E_{xm}(y,k)\\ H_{ym}(y,k)\\ H_{zm}(y,k)\end{pmatrix}\cos(k_{xm}x).$$

For each modal number k_{xm} we write an independent system of equations

$$\begin{aligned} -k_{xm}H_{zm} + i\frac{k}{\beta}H_{xm} &= i\omega\epsilon_0 E_{ym},\\ -i\frac{k}{\beta}H_{ym} - \frac{\partial}{\partial y}H_{zm} &= i\omega\epsilon_0 E_{xm},\\ \frac{\partial}{\partial y}H_{xm} + k_{xm}H_{ym} &= i\omega\epsilon_0 E_{zm} + v\rho_m\delta(y-y_0),\\ k_{xm}E_{zm} + i\frac{k}{\beta}E_{xm} &= -i\omega\mu_0 H_{ym},\\ -i\frac{k}{\beta}E_{ym} - \frac{\partial}{\partial y}E_{zm} &= -i\omega\mu_0 H_{xm},\\ \frac{\partial}{\partial y}(E_{xm}) - k_{xm}E_{ym} &= -i\omega\mu_0 H_{zm},\\ \frac{\partial}{\partial y}H_{ym} + k_{xm}H_{xm} - ikH_{zm} &= 0,\\ \frac{\partial}{\partial y}E_{ym} - k_{xm}E_{xm} - ikE_{zm} &= \frac{\rho_m}{\epsilon_0}. \end{aligned} \tag{30}$$

The surface impedance boundary condition, Eq. (1), takes the following form

$$\begin{pmatrix} E_{zm}(a)\\ -E_{xm}(a)\end{pmatrix} = \begin{pmatrix} Z_{TM} & Z_{12}\\ Z_{21} & Z_{TE}\end{pmatrix}\begin{pmatrix} H_{xm}(a)\\ H_{zm}(a)\end{pmatrix}. \tag{31}$$

It is well known that for a rectangular pipe the beam impedance can be written as expansion in the modal number k_{xm} [21]

$$Z_{\parallel}(x_0,y_0,x,y,k) = \frac{1}{w}\sum_{m=1}^{\infty}Z_m(y_0,y,k,\gamma)\sin(k_{xm}x_0)\sin(k_{xm}x) + Z_{sc}(x_0,y_0,x,y,k,\gamma), \tag{32}$$

$$Z_{sc}(x_0, y_0, x, y, k, \gamma) = \frac{1}{w}\sum_{m=1}^{\infty} Z_{sc,m}(y_0, y, k, \gamma)\sin(k_{xm}, x_0)\sin(k_{xm}x), \quad (33)$$

$$Z_{sc,m}(y_0, y, k, \gamma) = -\frac{ikZ_0}{2(\gamma^2-1)k_{ym}} e^{-k_{ym}|y_0-y|}, \qquad k_{ym} = \sqrt{k_{xm}^2+\nu^2}, \quad (34)$$

where the modal impedance reads

$$Z_m(y_0, y, k, \gamma) = Z_m^{cc}(k, \gamma)\cosh(k_{ym}y_0)\cosh(k_{ym}y) + Z_m^{ss}(k, \gamma)\sinh(k_{ym}y_0)\sinh(k_{ym}y). \quad (35)$$

Here $Z_{sc}(x_0, y_0, x, y, k, \gamma)$ is the impedance between the two vertical perfectly conducting plates at $x = 0$ and at $x = 2w$. In the limit when the coordinates of the perfectly conducting plates go to $\pm\infty$ it reduces to Z_{sc}^{∞}, Eq. (75).

From system of first-order equations, Eq. (30), we obtain the decoupled second-order ones

$$\frac{\partial^2}{\partial y^2}E_{zm} - k_{y,m}^2 E_{zm} = \frac{iq\delta(y-y_0)\nu^2}{\omega\epsilon_0}, \quad (36)$$

$$\frac{\partial^2}{\partial y^2}H_{zm} - k_{y,m}^2 H_{zm} = 0. \quad (37)$$

The longitudinal field components can be presented as sums of complex exponents

$$E_{zm}(r) = C_+^m e^{k_{ym}y} + C_-^m e^{-k_{ym}y}, \qquad H_{zm}(r) = D_+^m e^{k_{ym}y} + D_-^m e^{-k_{ym}y}. \quad (38)$$

Just as in case of round pipe of the previous section we numerate the electric field $E_{zm}(y)$ by index "0" for $y < y_0$ and by index "1" for $y > y_0$. The magnetic field $H_{zm}(y)$ has the same representation in the whole domain. If we integrate Eq. (36) from $y_0 - \Delta$ to $y_0 + \Delta$ and take limit for $\Delta \to 0$ then we obtain the jump in the derivative:

$$\frac{\partial}{\partial y}E_{zm}^1(y_0) - \frac{\partial}{\partial y}E_{zm}^0(y_0) = \frac{ik}{\gamma^2\beta\epsilon_0}\rho_m. \quad (39)$$

The term $Z_m^{cc}(k, \gamma)$ in Eq. (35) can be found from the solution of the problem in the half of the domain with magnetic boundary condition at the symmetry plane. From the condition $H_{zm}(0) = 0$, $H_{xm}(0) = 0$ we obtain $D_-^m = -D_+^m$, $C_-^{m,0} = C_+^{m,0}$.

At the position of the beam y_0 the longitudinal component E_z is continuous and we can write

$$2C_+^{m,0}\cosh(k_{ym}y_0) = C_+^{m,1}e^{k_{ym}y_0} + C_-^{m,1}e^{-k_{ym}y_0}. \quad (40)$$

The derivative of the field E_z has jump, Eq. (39), and from Eq. (38) we obtain

$$C_+^{m,1}e^{k_{ym}y_0} - C_-^{m,1}e^{-k_{ym}y_0} - 2C_+^{m,0}\sinh(k_{ym}y_0) = \frac{ik}{k_{y,m}\gamma^2\beta\epsilon_0}\rho_m. \quad (41)$$

Combining Eqs. (40) and (41) we can derive the relation

$$C_+^{m,1} - C_-^{m,1} = \frac{ik}{k_{ym}\gamma^2\beta\epsilon_0}\rho_m\cosh(k_{ym}y_0). \quad (42)$$

Hence the impedance term $Z_m^{cc}(k, \gamma)$ can be found as

$$Z_m^{cc}(k,\gamma) = \frac{E_{z,m}^1(y_0) - qZ_{sc,m}^{cc}(y_0)}{q\cosh(k_{ym}r_0)^2} = \frac{2C_I^{m,1}}{q\cosh(k_{ym}r_0)}, \quad (43)$$

where

$$Z_{sc,m}^{cc}(y_0) = [Z_{sc,m}(y_0, y_0, k, \gamma) + Z_{sc,m}(-y_0, y_0, k, \gamma)]/2. \quad (44)$$

In order to find the constants D_+^m, $C_+^{m,0}$, $C_+^{m,1}$, $C_-^{m,1}$, we use Eqs. (40), (42) and the impedance boundary condition, Eq. (31), where the transversal field components are defined through the longitudinal ones as

$$H_{xm}^1 = -\frac{ik}{\nu^2}\left(\frac{1}{Z_0}\frac{\partial}{\partial y}E_{zm}^1 + \frac{k_{xm}}{\beta}H_{zm}\right), \quad (45)$$

$$E_{xm}^1 = \frac{ik}{\nu^2}\left(Z_0\frac{\partial}{\partial y}H_{zm} + \frac{k_{xm}}{\beta}E_{zm}^1\right). \quad (46)$$

From straightforward symbolic calculations [20] we find out that the impedance term $Z_m^{cc}(k, \gamma)$ can be written as

$$Z_m^{cc}(k,\gamma) = \frac{Z_{\mathrm{TM}}N}{D} + Z_{\mathrm{pipe},m}^{cc}(k,\gamma), \quad (47)$$

$$N = k_{ym} - \frac{ik}{\beta^2\gamma^2}\frac{|\boldsymbol{Z}^s|}{Z_0 Z_{\mathrm{TM}}}\tanh(ak_{ym}), \quad (48)$$

$$D = -iA\sinh(2ak_{ym}) + \frac{|\boldsymbol{Z}^s|}{Z_0^2}2k_{ym}\sinh^2(ak_{ym}) + 2k_{ym}\cosh^2(ak_{ym}), \quad (49)$$

$$A = \frac{\gamma^2 Z_{\mathrm{TM}}(k_{xm}^2 - \beta^2 k_{ym}^2)}{kZ_0} + \frac{i(Z_{12} - Z_{21})k_{xm}}{\beta Z_0} + \frac{kZ_{\mathrm{TE}}}{\beta^2\gamma^2 Z_0}, \quad (50)$$

$$Z_{\mathrm{pipe},m}^{cc}(k,\gamma) = \frac{ikZ_0[1 - \tanh(ak_{ym})]}{2\gamma^2\beta^2 k_{ym}}. \quad (51)$$

Here $Z^{cc}_{\mathrm{pipe},m}(k,\gamma)$ is the modal impedance of nonrelativistic charge in perfectly conducting rectangle with the magnetic boundary condition at the symmetry plane, $y=0$.

In the same way the item $Z^{ss}_m(k,\gamma)$ can be found from the solution of the problem in the half of the domain with electric boundary condition at the symmetry plane. From the equations $E_{zm}(0)=0$, $E_{xm}(0)=0$ we obtain $D^m_-=D^m_+$, $C^{m,0}_-=-C^{m,0}_+$.

At the position of the beam y_0 the longitudinal component E_z is continuous and we can write

$$2C^{m,0}_+\sinh(k_{ym}y_0)=C^{m,1}_+e^{k_{ym}y_0}+C^{m,1}_-e^{-k_{ym}y_0}. \tag{52}$$

From the jump of the derivative of E_z at y_0 we obtain

$$C^{m,1}_++C^{m,1}_-=\frac{ik}{k_{ym}\gamma^2\beta\epsilon_0}\rho_m\sinh(k_{ym}y_0). \tag{53}$$

Hence the impedance term $Z^{ss}_m(k,\gamma)$ can be found as

$$Z^{ss}_m(k,\gamma)=\frac{E^1_{zm}(r_0)-qZ^{ss}_{sc,m}}{q\sinh(k_{ym}r_0)^2}=\frac{2C^{m,1}_I}{q\ \sinh(k_{ym}r_0)}, \tag{54}$$

where

$$Z^{ss}_{sc,m}=[Z_{sc,m}(y_0,y_0,k,\gamma)-Z_{sc,m}(-y_0,y_0,k,\gamma)]/2. \tag{55}$$

Following the same route of derivation as for $Z^{cc}_m(k,\gamma)$ we obtain the impedance term $Z^{ss}_m(k,\gamma)$:

$$Z^{ss}_m(k,\gamma)=\frac{Z_{\mathrm{TM}}N}{D}+Z^{cc}_{\mathrm{pipe},m}(k,\gamma), \tag{56}$$

$$N=k_{y,m}-\frac{ik}{\beta^2\gamma^2}\frac{|\boldsymbol{Z}^s|}{Z_0Z_{\mathrm{TM}}}\coth(ak_{ym}) \tag{57}$$

$$D=-iA\ \sinh(2ak_{ym})+\frac{|\boldsymbol{Z}^s|}{Z_0^2}2k_{ym}\cosh^2(ak_{ym})+2k_{ym}\sinh^2(ak_{ym}), \tag{58}$$

$$Z^{ss}_{\mathrm{pipe},m}(k,\gamma)=\frac{ikZ_0(\coth(ak_{ym})-1)}{2\beta^2\gamma^2k_{ym}}. \tag{59}$$

Here $Z^{ss}_{\mathrm{pipe},m}(k,\gamma)$ is the modal impedance of nonrelativistic charge in perfectly conducting rectangle with the electric boundary condition at the symmetry plane, $y=0$.

In the relativistic limit, $\gamma\to\infty$, the equations reduce to the following expressions

$$Z_m(y_0,y,k)=Z^{cc}_m(k)\ \cosh(k_{xm}y_0)\ \cosh(k_{xm}y)+Z^{ss}_m(k)\ \sinh(k_{xm}y_0)\ \sinh(k_{xm}y), \tag{60}$$

$$Z^{cc}_m(k)=\frac{Z_{\mathrm{TM}}}{2\frac{|\boldsymbol{Z}^s|}{Z_0^2}\sinh^2(ak_{xm})+B\sinh(2ak_{xm})+2\cosh^2(ak_{xm})}, \tag{61}$$

$$Z^{ss}_m(k)=\frac{Z_{\mathrm{TM}}}{2\frac{|\boldsymbol{Z}^s|}{Z_0^2}\cosh^2(ak_{xm})+B\sinh(2ak_{xm})+2\sinh^2(ak_{xm})}, \tag{62}$$

where

$$B=\frac{Z_{12}-Z_{21}}{Z_0}+i\frac{Z_{\mathrm{TM}}}{Z_0}\left(\frac{k}{k_{x,m}}-\frac{k_{x,m}}{k}\right). \tag{63}$$

C. One plate with surface impedance placed between two perfectly conducting sidewalls

Let us consider the case when there is only one plate with the impedance boundary condition placed at $y=0$ as shown in Fig. 1. The charge is at the position $y_0<0$.

The beam impedance has the same form given by Eq. (32) but the modal impedance has different representation

$$Z_m(y_0,y,k,\gamma)=Z_m(k,\gamma)e^{k_{ym}(y_0+y)}. \tag{64}$$

The electric and magnetic longitudinal fields components are presented by the same form, Eq. (38), as for the rectangular pipe. To avoid divergence of the field at $y=-\infty$ we have to put $C^{m,0}_-=0$, $D^m_-=0$. Again the $H_{zm}(y)$ component has the same representation in the whole domain and we are looking only for the constants $C^{m,0}_+$, $C^{m,1}_+$, $C^{m,1}_-$, D^m_+. From four equations

$$\begin{aligned}E^1_{zm}(0)&=Z_{TM}H^1_{xm}(0)+Z_{12}H_{zm}(0),\\ E^1_{xm}(0)&=-Z_{TE}H_{zm}(0)-Z_{21}H^1_{xm}(0),\end{aligned} \tag{65}$$

$$\begin{aligned}E^0_{zm}(y_0)&=E^1_{zm}(y_0),\\ \frac{\partial}{\partial y}E^1_{zm}(y_0)-\frac{\partial}{\partial y}E^0_{zm}(y_0)&=\frac{ik}{\gamma^2\beta\epsilon_0}\rho_m,\end{aligned} \tag{66}$$

we obtain the four constants straightforwardly.

The impedance term will be obtained from the relation

$$Z_m(k,\gamma)=\frac{E^1_{zm}(y_0)-qZ_{sc,m}}{qe^{2k_{ym}y_0}}=\frac{C^{m,1}_+}{qe^{k_{ym}y_0}}. \tag{67}$$

Hence the modal beam impedance of Π-shaped waveguide reads

$$Z_m(k,\gamma)=\frac{Z_{\mathrm{TM}}N}{D}+Z_{\mathrm{pipe},m}(k,\gamma), \tag{68}$$

$$N = k_{y,m} - \frac{ik|\boldsymbol{Z}^s|}{\beta^2\gamma^2 Z_0 Z_{\mathrm{TM}}}, \tag{69}$$

$$D = \left(\frac{|\boldsymbol{Z}^s|}{Z_0^2} + 1\right)k_{ym} + k_{xm}\left(\frac{Z_{12} - Z_{21}}{\beta Z_0} - \frac{i\gamma^2 Z_{\mathrm{TM}} k_{xm}}{kZ_0}\right) + \frac{i\beta^2\gamma^2 Z_{\mathrm{TM}} k_{ym}^2}{kZ_0} - \frac{ikZ_{\mathrm{TE}}}{\beta^2\gamma^2 Z_0}, \tag{70}$$

$$Z_{\mathrm{pipe},m}(k,\gamma) = \frac{ikZ_0}{2\beta^2\gamma^2 k_{ym}}. \tag{71}$$

Here $Z_{\mathrm{pipe},m}(k,\gamma)$ is the modal impedance of nonrelativistic charge in perfectly conducting Π-shaped structure.

In the relativistic limit, $\gamma \to \infty$, the previous equations reduce to the following expressions

$$Z_m(y_0, y, k) = Z_m(k)e^{k_{xm}(y_0+y)}, \tag{72}$$

$$Z_m(k) = \frac{Z_{\mathrm{TM}}}{1 + i\frac{Z_{\mathrm{TM}}}{Z_0}\left(\frac{k}{k_{xm}} - \frac{k_{xm}}{k}\right) + \frac{|\boldsymbol{Z}^s|}{Z_0^2} - \frac{Z_{21}-Z_{12}}{Z_0}}. \tag{73}$$

D. Infinite and semi-infinite plates

In the case of infinite plates, $-\infty < x < \infty$, the impedance reads

$$Z_{\parallel}(x_0, y_0, x, y, k) = \frac{1}{\pi}\int_0^\infty Z(y_0, y, k, k_x, \gamma)\cos(k_x(x_0 - x))dk_x + Z_{sc}^{\infty}(x_0, y_0, x, y, k, \gamma), \tag{74}$$

$$Z_{sc}^{\infty}(x_0, y_0, x, y, k, \gamma) = -\frac{kZ_0}{2\pi(\gamma^2 - 1)}K_0\left(\frac{k\sqrt{(x - x_0)^2 + (y - y_0)^2}}{\gamma\beta}\right), \tag{75}$$

where $Z(y_0, y, k, k_x, \gamma)$ is defined by Eq. (35) for two parallel plates or by Eq. (64) for one plate.

In the case of semi-infinite plates, $0 \le x < \infty$, the impedance reads

$$Z_{\parallel}(x_0, y_0, x, y, k) = \frac{2}{\pi}\int_0^\infty Z(y_0, y, k, k_x, \gamma)\,\sin(k_x x_0)\,\sin(k_x x)dk_x + Z_{sc}^{\mathrm{semi}}(x_0, y_0, x, y, k, \gamma),$$
$$Z_{sc}^{\mathrm{semi}}(x_0, y_0, x, y, k, \gamma) = Z_{sc}^{\infty}(x_0, y_0, x, y, k, \gamma) - Z_{sc}^{\infty}(-x_0, y_0, x, y, k, \gamma), \tag{76}$$

where again $Z(y_0, y, k, k_x, \gamma)$ is defined by Eq. (35) for two parallel plates or by Eq. (64) for one plate.

III. MANY HOMOGENEOUS LAYERS CLOSED BY PIPE WITH SURFACE IMPEDANCE

In this section we describe modification of the field matching method published in [18,19] to include an impedance boundary condition. Additionally we consider the case of Π-shaped structure which was not analyzed before.

Let us consider a round pipe sketched in Fig. 2 with many layers possessing the uni-axial anisotropy. It means that the permittivity and the permeability tensors are diagonal and for their elements the following relations hold

$$\epsilon_r(r) = \epsilon_\varphi(r), \qquad \mu_r(r) = \mu_\varphi(r).$$

We do not have to assume any particular frequency dependence. In order to include conductivity and other losses in numerical code we use the following expressions (here we consider as example the r-component):

$$\epsilon_r(r,k) = \epsilon_r'(r)[1 - i\delta_r^\epsilon(r)] - i\frac{\sigma_c(r)}{\omega[1 + i\omega\tau(r)]},$$
$$\mu_r(r,k) = \mu_r'(r)[1 - i\delta_r^\mu(r)], \qquad \omega = kc, \tag{77}$$

where ϵ_r' is the real part of the complex permittivity, μ_r' is the real part of the complex permeability, and the loss can be introduced with the help of dielectric loss tangent δ_r^ϵ, magnetic loss tangent δ_r^μ or/and with ac conductivity following the Drude model [1], where σ_c is the dc conductivity of the material and τ its relaxation time. We use similar expressions for z- components of the permittivity and the permeability tensors.

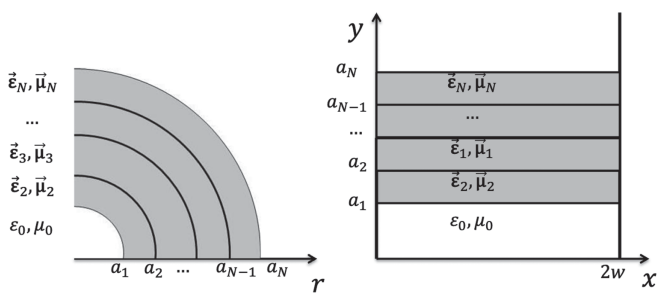

FIG. 2. Transverse to z-axis cross sections of "round" and "rectangular" layered pipes.

Inside of each layer where the complex permeability and permittivity are constants (independent from r) a general solution can be written in form similar to Eq. (11)

$$\begin{aligned} E_{zm}(r) &= C_I^m I_m(\nu_r^\epsilon r) + C_K^m K_m(\nu_r^\epsilon r), \\ H_{zm}(r) &= D_I^m I_m(\nu_r^\mu r) + D_K^m K_m(\nu_r^\mu r), \\ \nu_r^\epsilon &= \nu_r\sqrt{\epsilon_z/\epsilon_r}, \\ \nu_r^\mu &= \nu_r\sqrt{\mu_z/\mu_r}, \\ \nu_r^2 &= k^2\beta^{-2} - \omega^2\epsilon_r\mu_r, \end{aligned} \tag{78}$$

where I_m, K_m are modified Bessel functions of complex argument.

In the following we will numerate the layers by index j and $r = a_j$ defines interface between the layers with numbers j and $j+1$. In order to find the constants $C_I^{m,j}, C_K^{m,j}, D_I^{m,j}, D_K^{m,j}$ in Eq. (78) we use four conditions at the interfaces between the layers:

$$\begin{aligned} E_{zm}^j(a_j) = E_{zm}^{j+1}(a_j), \qquad H_{zm}^j(a_j) = H_{zm}^{j+1}(a_j), \\ \epsilon_r^j E_{rm}^j(a_j) = \epsilon_r^{j+1} E_{rm}^{j+1}(a_j), \quad \mu_r^j H_{rm}^j(a_j) = \mu_r^{j+1} H_{rm}^{j+1}(a_j), \end{aligned} \tag{79}$$

where the radial field components are defined through the longitudinal ones as

$$\begin{aligned} E_{rm}^j(r) &= \frac{ik}{\nu_r^2}\left(\frac{1}{\beta}\frac{\partial}{\partial r}E_{mz}^j + \frac{mc\mu_r}{r}H_{zm}\right), \\ H_{rm}^j(r) &= \frac{ik}{\nu_r^2}\left(\frac{1}{\beta}\frac{\partial}{\partial r}H_{mz}^j + \frac{mc\epsilon_r}{r}E_{zm}\right). \end{aligned} \tag{80}$$

From Eqs. (78)–(80) at each interface $r = a_j$ we obtain the relations

$$\begin{aligned} &\left(C_I^{m,j+1}, C_K^{m,j+1}, D_I^{m,j+1}, D_K^{m,j+1}\right)^T \\ &\quad = \mathbf{M}_j\left(C_I^{m,j}, C_K^{m,j}, D_I^{m,j}, D_K^{mj,}\right)^T, \end{aligned} \tag{81}$$

where $\mathbf{M}_j$ is a complex matrix of order 4. The explicit expressions for the elements of matrix $\mathbf{M}_j$ are given in Appendix A. They can be written as a combination of modified Bessel functions and the expressions are similar to those obtained in [18] for an isotropic case.

The matrix connecting the coefficients from vacuum layer to the coefficients of the last layer can be found as a matrix product

$$\hat{\mathbf{M}} = \mathbf{M}_{N-1}\mathbf{M}_{N-2}\ldots\mathbf{M}_1.$$

The last layer, $j = N$, is closed with pipe at $r = a_N$ described by surface impedance, Eq. (5). Hence in order to take into the account the impedance boundary condition we have to find the matrix

$$\mathbf{M} = \mathbf{M}_N^{C2F}\hat{\mathbf{M}},$$

where $\mathbf{M}_N^{C2F}$ is a matrix converting the field coefficients into the field components:

$$\begin{pmatrix} E_{z,m}(a_N) \\ H_{z,m}(a_N) \\ E_{\varphi,m}(a_N) \\ H_{\varphi,m}(a_N) \end{pmatrix} = \mathbf{M}_N^{C2F}\begin{pmatrix} C_I^{m,N} \\ C_K^{m,N} \\ D_I^{m,N} \\ D_K^{m,N} \end{pmatrix}. \tag{82}$$

The explicit form of the elements of the matrix $\mathbf{M}_N^{C2F}$ is given in Appendix A.

From the boundary condition at the axis we obtain $D_K^{m,1} = 0$. The coefficient $C_K^{m,1}$ is known and given by Eq. (15). Hence we are looking for the solution of the following simple system:

$$\begin{pmatrix} M_{11} & M_{13} & Z_{12} & Z_{TM} \\ M_{21} & M_{23} & -1 & 0 \\ M_{31} & M_{33} & -Z_{TE} & -Z_{21} \\ M_{41} & M_{43} & 0 & -1 \end{pmatrix}\begin{pmatrix} C_I^{m,1}/C_K^{m,1} \\ D_I^{m,1}/C_K^{m,1} \\ H_{z,m}^N/C_K^{m,1} \\ H_{\varphi,m}^N/C_K^{m,1} \end{pmatrix} = \begin{pmatrix} -M_{12} \\ -M_{22} \\ -M_{32} \\ -M_{42} \end{pmatrix}. \tag{83}$$

After numerically solving of Eq. (83) the modal longitudinal impedance in Eq. (7) can be found as

$$Z_m(k,\gamma) = -\frac{ikZ_0}{\delta_{m0}\pi(\gamma^2-1)}\frac{C_I^{m,1}}{C_K^{m,1}}.$$

For rectangular geometries sketched in Fig. 2 we follow the same approach and the same suggestion of uniaxial anisotropy (transverse permeability and permittivity are different from the longitudinal ones). The field in the homogeneous uniaxially anisotropic layer can be presented as sum of complex exponents

$$\begin{aligned} E_{zm}(r) &= C_+^m e^{k_{ym}^\epsilon y} + C_-^m e^{-k_{ym}^\epsilon y}, \\ H_{zm}(r) &= D_+^m e^{k_{ym}^\mu y} + D_-^m e^{-k_{ym}^\mu y}, \\ k_{ym}^\epsilon &= \sqrt{k_{xm}^2 + \nu_y^2\frac{\epsilon_z}{\epsilon_y}}, \\ k_{ym}^\mu &= \sqrt{k_{xm}^2 + \nu_y^2\frac{\mu_z}{\mu_y}}, \\ \nu_y^2 &= k^2\beta^{-2} - \omega^2\epsilon_y^2\mu_y^2. \end{aligned} \tag{84}$$

In the following we consider only the case where the rectangular structure is symmetric in the y-direction (up-bottom symmetry). In this case Eq. (35) for the modal impedance $Z_m(y_0, y, k, \gamma)$ holds. The item $Z_m^{cc}(k, \gamma)$ can be found from the solution of the problem in the half of the domain with magnetic boundary condition at the symmetry plane $H_{z,m}(0) = 0$. Hence we are looking for the solution of the following system:

$$\begin{pmatrix} M_{11}+M_{12} & M_{13}-M_{14} & -Z_{12} & -Z_{TM} \\ M_{21}+M_{22} & M_{23}-M_{24} & -1 & 0 \\ M_{31}+M_{32} & M_{33}-M_{34} & Z_{TE} & -Z_{21} \\ M_{41}+M_{42} & M_{43}-M_{44} & 0 & -1 \end{pmatrix} \begin{pmatrix} C_+^{m,0}/(C_-^{m,1}-C_+^{m,1}) \\ D_+^{m,0}/(C_-^{m,1}-C_+^{m,1}) \\ H_{z,m}^N/(C_-^{m,1}-C_+^{m,1}) \\ H_{x,m}^N/(C_-^{m,1}-C_+^{m,1}) \end{pmatrix} = \begin{pmatrix} -M_{12} \\ -M_{22} \\ -M_{32} \\ -M_{42} \end{pmatrix}, \tag{85}$$

where elements of the matrix are described in Appendix B.

After numerical solution of Eq. (85) the item $Z_m^{cc}(k, \gamma)$ can be found as

$$Z_m^{cc}(k, \gamma) = -\frac{2ikZ_0}{(\gamma^2-1)k_{y,m}^0} \frac{C_+^{m,1}}{(C_-^{m,1}-C_+^{m,1})}, \qquad k_{y,m}^0 = \sqrt{k_{x,m}^2 + \frac{k^2}{\gamma^2\beta^2}}.$$

The item $Z_m^{ss}(k, \gamma)$ can be found from the solution of another problem in the half of the domain with electric boundary condition at the symmetry plane $E_{z,m}(0) = 0$. We are looking for the solution of the following system:

$$\begin{pmatrix} M_{11}-M_{12} & M_{13}+M_{14} & -Z_{12} & -Z_{TM} \\ M_{21}-M_{22} & M_{23}+M_{24} & -1 & 0 \\ M_{31}-M_{32} & M_{33}+M_{34} & Z_{TE} & Z_{21} \\ M_{41}-M_{42} & M_{43}+M_{44} & 0 & -1 \end{pmatrix} \begin{pmatrix} C_+^{m,0}/(C_-^{m,1}+C_+^{m,1}) \\ D_+^{m,0}/(C_-^{m,1}+C_+^{m,1}) \\ H_{z,m}^{m,N}/(C_-^{m,1}+C_+^{m,1}) \\ H_{x,m}^{m,N}/(C_-^{m,1}+C_+^{m,1}) \end{pmatrix} = \begin{pmatrix} -M_{12} \\ -M_{22} \\ -M_{32} \\ -M_{42} \end{pmatrix}. \tag{86}$$

After numerical solution of Eq. (86) the item $Z_m^{ss}(k, \gamma)$ can be found as

$$Z_m^{ss}(k, \gamma) = -\frac{2ikZ_0}{(\gamma^2-1)k_{y,m}^0} \frac{C_+^{m,1}}{(C_-^{m,1}+C_+^{m,1})}.$$

Finally let us consider only one plate with the same structure of layers as shown in Fig. 2. We use Eq. (64) for the modal impedance $Z_m(y_0, y, k, \gamma)$ and Eq. (84) for the longitudinal field components. In order to avoid the divergence of the fields at $y = -\infty$ we have to put $D_-^{m,1} = 0$. Hence we are looking for the solution of the following system:

$$\begin{pmatrix} M_{11} & M_{13} & -Z_{12} & -Z_{TM} \\ M_{21} & M_{23} & -1 & 0 \\ M_{31} & M_{33} & Z_{TE} & Z_{21} \\ M_{41} & M_{43} & 0 & -1 \end{pmatrix} \begin{pmatrix} C_+^{m,1}/C_-^{m,1} \\ D_+^{m,1}/(C_-^{m,1} \\ H_{z,m}^N/C_-^{m,1} \\ H_{x,m}^N/C_-^{m,1} \end{pmatrix} = \begin{pmatrix} -M_{12} \\ -M_{22} \\ -M_{32} \\ -M_{42} \end{pmatrix}, \tag{87}$$

where elements of the matrix $\mathbf{M} = \mathbf{M}_N^{C2F}\hat{\mathbf{M}}$ are the same as for the rectangular case and described in Appendix B.

After numerical solution of Eq. (87) the item $Z_m(k, \gamma)$ can be found as

$$Z_m(k, \gamma) = -\frac{ikZ_0}{(\gamma^2-1)k_{y,m}^0} \frac{C_+^{m,1}}{C_-^{m,1}}. \tag{88}$$

IV. APPLICATIONS

In this section we consider several examples of the application of the analytical techniques described in the paper to the real structures with corrugations, dielectrics, and anomalous skin effects. We consider only the relativistic limit $\gamma \to \infty$.

A. Short-range wakes of corrugated structures

In this section we consider corrugated structures sketched in Fig. 3: rectangular and round corrugated waveguides. The corrugations have period p and gap t, which is smaller than the gap depth h.

The short-range wakefields of two corrugated plates have been analyzed in [6,7]. These studies have established that the surface impedance formalism can be employed

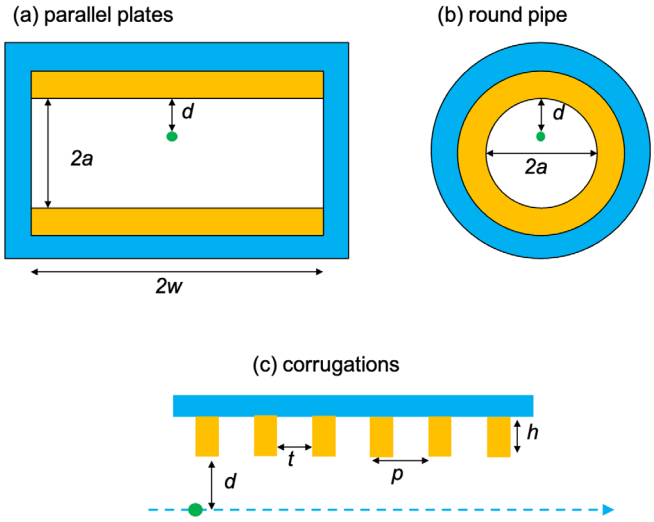

FIG. 3. Sketches of rectangular (a) and round (b) structures in front view with corrugations as yellow layers. The parameters of the corrugations are shown in side view (c). The point charge position is shown by green circle.

under the condition that the gap depth h exceeds the gap width t, and the distance to the wall d is greater than the corrugation period p.

The approximations for one corrugated plate are obtained in [8] in the limit $a \to \infty$. Let us give a more accurate formulas for the case of one infinite plate for arbitrary offsets of the source and the witness particles.

As shown in [7,22] the corrugations can be described by surface impedance

$$Z_{\mathrm{TM}}(k) = Z_0 \frac{1+i}{\sqrt{k s_c}}, \qquad s_c = \frac{\pi}{t}(\alpha(t/p)p)^2,$$
$$\alpha(x) = -0.07x - 0.465\sqrt{x} + 1. \tag{89}$$

We take the surface impedance $Z_{\mathrm{TE}}(k) \equiv 0$, since the surface currents in horizontal direction are not impeded by the corrugations [12]. If we additionally assume that $k \gg k_x$, then the modal impedance, Eq. (73), can be approximated as

$$Z(k, k_x) = \frac{Z_{\mathrm{TM}}}{1 + \frac{ik}{k_x}\frac{Z_{\mathrm{TM}}}{Z_0}}. \tag{90}$$

The modal wake function of point charge is given by the inverse Fourier transform of the impedance

$$w(s, k_x) = Z_0 c k_x e^{s/\bar{s}(k_x)} \operatorname{erfc}[\sqrt{s/\bar{s}(k_x)}], \qquad \bar{s}(k_x) \frac{2}{s_c k_x^2}, \tag{91}$$

and for s small compared to $\bar{s}(k_x)$ Eq. (91) can be approximated by exponential function [7]

$$w(s, k_x) = Z_0 c k_x e^{-k_x\sqrt{s s_c/2}}. \tag{92}$$

Integrating in k_x we obtain the longitudinal wake function for arbitrary offsets of the source and the witness particles:

$$w_{\parallel}(x_0, y_0, x, y, s)$$
$$= \frac{Z_0 c}{\pi}\int_0^{\infty} e^{-k_x(\sqrt{0.5 s s_c} - y_0 - y)} \cos[k_x(x - x_0)] dk_x$$
$$= \frac{Z_0 c}{\pi}\frac{(\sqrt{0.5 s s_c} - y_0 - y)^2 - (x - x_0)^2}{\left[(\sqrt{0.5 s s_c} - y_0 - y)^2 + (x - x_0)^2\right]^2}, \tag{93}$$

where (x_0, y_0) are the transverse coordinates of the source particle, (x, y) are the transverse coordinates of the witness particle, and s is the distance between them. For the same horizontal offset of both particles, $x = x_0$, the vertical component of the transverse wake function reads

$$w_y(y_0, y, s) = \frac{Z_0 c}{\pi}\frac{2s}{(-y - y_0)(\sqrt{0.5 s s_c} - y_0 - y)^2}, \tag{94}$$

and the monopole component of the transverse wake ($y = y_0$) can be written in the form

$$w_y(y_0, s) = \frac{Z_0 c}{\pi}\frac{s}{y_0(\sqrt{0.5 s s_c} - 2y_0)^2}. \tag{95}$$

In order to confirm the accuracy of the obtained equations we consider an example of plates with the corrugation parameters from Table I. We consider a rectangular waveguide with relatively large aperture, $2a = 4$ mm, and large width, $2w = 12$ mm. The Gaussian bunch with longitudinal density $\lambda(s)$ of rms length $\sigma_z = 10$ μm has offset from the symmetry axis equal to 1.5 mm. It means that the short-range wake potential of such bunch is equal to the short-range wake potential of the same bunch flying with offset $y_0 = 0.5$ mm from one infinite plate. The correctness of this assumption for the given case was confirmed in [23]. The wake potential at this offset is obtained numerical with code ECHO [21] through the modal expansion similar to Eq. (32):

TABLE I. Corrugations parameters used in the calculations.

Parameter	Value	Units
Period, p	0.5	mm
Longitudinal gap, t	0.25	mm
Depth, h	0.5	mm
Nominal distance to the wall, d	0.5	mm
Aperture (diameter), $2a$	4	mm
Width, $2w$	12	mm

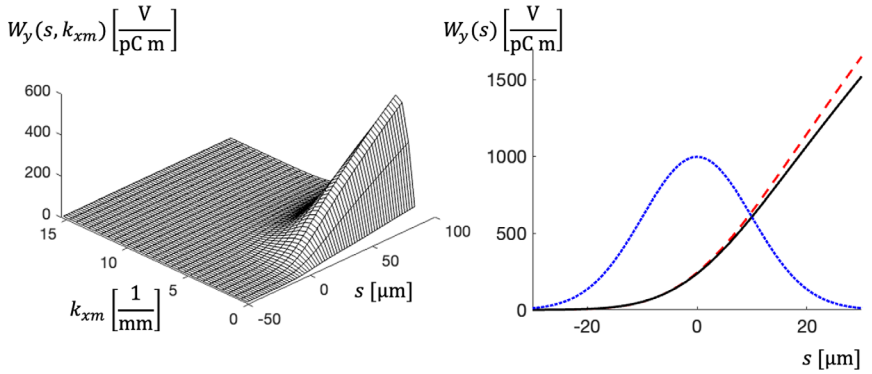

FIG. 4. Transverse wake potential of corrugated plate for the Gaussian bunch with rms length of 10 μm moving at 0.5 mm offset from the plate. The left plot shows dependence of the modal wake potential $W_y(s,k_{xm})$ from the modal number k_{xm} as calculated by ECHO [21]. The right plot compares the numerical result from ECHO (solid line) with the wake potential calculated from Eq. (95) (red dashed curve).

$$W_y(s)=\sum_{m=1}^{40}W_y(s,k_{xm})\sin^2\left(\frac{\pi m}{2}\right),\quad k_{xm}=\frac{\pi m}{2w}. \tag{96}$$

The left plot in Fig. 4 shows dependence of the modal wake potential $W_y(s,k_{xm})$ from the modal number k_{xm}. The maximal contribution is done by the mode with the modal number $k_{x7}=1.83\ \mathrm{mm}^{-1}$. The right plot in Fig. 4 compares the numerical result from ECHO (solid line) with the wake potential calculated from Eq. (95) and we see only small difference between the curves in the plot.

The characteristic wave number for this Gaussian beam can be estimated as $k=1/\sigma_z=100\ \mathrm{mm}^{-1}$. The left plot confirms that at the beam offset of 0.5 mm from the plate the condition $k_x \ll k$ holds for the modal numbers k_x which contribute to the wake potential.

The wake potential for the given wake function $w(s)$ and a normalized charge distribution $\lambda(s)$ was obtained by convolution

$$W_{||}(s)=\int_0^\infty w_{||}(s')\lambda(s-s')ds'. \tag{97}$$

In order to confirm accuracy of the exponential approximation, Eq. (92), we have compared in the left plot of Fig. 5 the curves from Eq. (91) (solid black line) and Eq. (92) (dashed red curve) for the mode with the modal number k_{x7}, which makes the largest contribution to the wake potential [see Eq. (96)]. The right plot in Fig. 5 compares the curve from Eq. (95) (dashed red line) with the exponential approximation obtained in paper [8] (dotted blue line)

$$w_y(y_0)=\frac{Z_0c}{2\pi y_0^3}s_m(y_0)\left(1-\left(\sqrt{\frac{s}{s_m(y_0)}}+1\right)e^{-\sqrt{\frac{s}{s_m(y_0)}}}\right),$$
$$s_m(y_0)=\frac{8y_0^2}{9s_c}. \tag{98}$$

The solid black line presents the wake function obtained from Eq. (91) without exponential approximation. We conclude that Eq. (95) gives a better approximation of the "true" wake function in comparison with Eq. (98) published in [8].

As a next example let us consider a round pipe of radius a with corrugations along axis z. Following the same

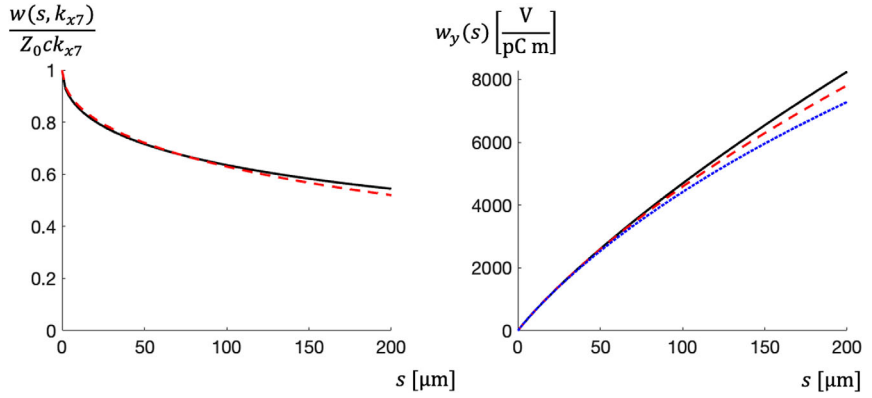

FIG. 5. The left plot compares the curves from Eq. (91) (solid black line) and Eq. (92) (dashed red curve). The right plot compares the curve from Eq. (95) (dashed red line) with the exponential approximation from [8], Eq. (98) (dotted blue line). The solid black line presents the wake function obtained from Eq. (91) without exponential approximation.

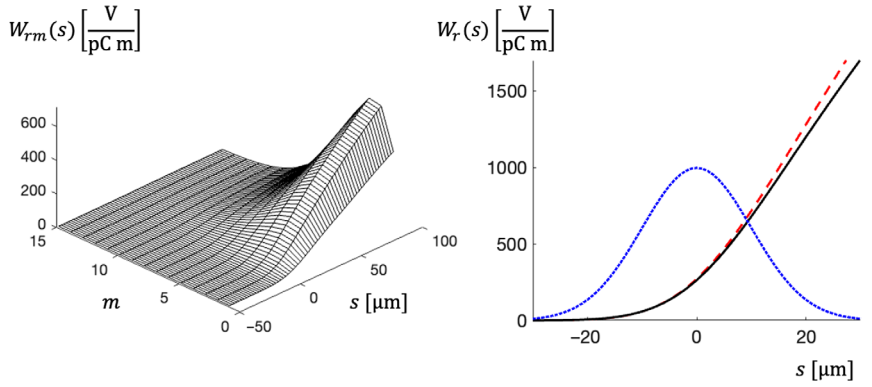

FIG. 6. Transverse wake potential of round corrugated pipe for the Gaussian bunch with rms length of 10 μm moving at 0.5 mm offset from the wall. The left plot shows the dependence of the modal wake potential $W_{rm}(s)$ from the modal number m as calculated by ECHO [21]. The right plot compares the numerical result from ECHO (solid line) with the wake potential calculated from Eq. (102) (red dashed curve).

arguments as in previous example we assume that $Z_{TE}(k) \equiv 0$. If we additionally assume that $m \ll ka$, then the modal impedance can be written as

$$Z_m(k) = \frac{Z_{\mathrm{TM}}}{a^{2m+1}\pi\left(1 + \delta_{m0} + \frac{iak}{m+1}\frac{Z_{\mathrm{TM}}}{Z_0}\right)}. \tag{99}$$

The modal wake function of point charge is given by the inverse Fourier transform of the impedance

$$w_m(s) = \frac{(m+1)Z_0 c}{\pi a^{2(m+1)}} e^{s/s_m}\mathrm{erfc}\left(\sqrt{s/s_m}\right),$$
$$s_m = \frac{2a^2}{s_c(m+1)^2(1+\delta_{m0})^2}. \tag{100}$$

For s small compared to s_m Eq. (99) can be approximated by the exponential function [7]

$$w_m(s) = \frac{(m+1)Z_0 c}{\pi a^{2(m+1)}} e^{-\sqrt{s/s_m}}. \tag{101}$$

For arbitrary offsets of the source and the witness particles the longitudinal wake function can be written as

$$w_{\parallel}(r_0, \varphi_0, r, \varphi, s) = \sum_{m=0}^{\infty} w_m(s) r_0^m r^m \cos\left[m(\varphi - \varphi_0)\right],$$

where (r_0, φ_0) are the transverse coordinates of the source particle, (r, φ) are the transverse coordinates of the witness particle, and s is the distance between them.

With the exponential approximation, Eq. (101), the radial component of the transverse wake function reads

$$w_r(r_0, \varphi_0, r, \varphi, s) = \sum_{m=1}^{\infty} m w_{rm}(s) r_0^m r^{m-1} \cos[m(\varphi - \varphi_0)], \tag{102}$$

$$w_{rm}(s) = -\int_{-\infty}^{s} w_m(x)dx$$
$$\approx -\frac{2(m+1)Z_0 c s_m}{\pi a^{2(m+1)}}\left(1 - \left(1 + \sqrt{s/s_m}\right)e^{-\sqrt{s/s_m}}\right). \tag{103}$$

The number of the modes required in the sum increases as the beam trajectory nears the wall. In the vicinity of the wall the used approximation fails as the condition $m \ll ka$ is violated.

In order to confirm applicability of the obtained approximation we have calculated the transverse wake potential for round pipe with the corrugation parameters listed in Table I for the Gaussian bunch $\lambda(s)$ with rms length $\sigma = 10$ μm and offset $r_0 = 1.5$ mm. The wake potential at this offset is obtained numerical with code ECHO through the modal expansion similar to Eq. (26):

$$W_r(s) = \sum_{m=1}^{20} W_{rm}(s). \tag{104}$$

The left plot in Fig. 6 shows dependence of the modal wake potential $W_{rm}(s)$ from the modal number m. The maximal contribution is done by the mode with the modal number $m = 4$. The right plot compares the numerical result from ECHO (solid line) with the wake potential calculated from Eq. (102) and we see only small difference between the curves.

The characteristic wave number for this Gaussian beam can be estimated as $k = 1/\sigma_z = 100\ \mathrm{mm}^{-1}$ and radius of the structure is $a = 2$ mm. The left plot confirms that at the beam offset $r_0 = 1.5$ from the symmetry axis the condition $m \ll ka$ holds for the modal numbers m which contribute to the wake potential.

B. Resistive wall wakes at cryogenic temperatures

Resistive wall wakefields generated due to finite conductivity of an accelerator vacuum chamber play an important role in beam dynamics and free electron laser physics. They are important for small apertures and short bunches used in modern undulators. For the metal surfaces at cryogenic temperatures the anomalous skin effect regime (ASE) has to be considered. The surface impedance of ASE reads [9]

$$\begin{aligned} Z_s(k) &= -Z_0 i \frac{kl}{F}, \\ F &= -\frac{u}{\pi}\cdot\int_0^\infty \log\left(1+\frac{\eta+\zeta\cdot\kappa(t)}{t^2}\right)dt, \\ \kappa(t) &= \frac{2}{t^3}[(1+t^2)\arctan(t)-t], \\ \eta &= -\left(\frac{kl}{u}\right)^2, \qquad \zeta = i\frac{\alpha}{u^3}, \\ u &= 1+ick\tau, \qquad \alpha = \frac{3}{2}\left(\frac{l}{\delta}\right)^2, \\ \delta &= \sqrt{\frac{2}{Z_0\sigma_c k}}, \qquad l = \tau v_f, \end{aligned} \tag{105}$$

where σ_c is the metal conductivity, v_f is the Fermi velocity, τ is the relaxation time.

Conductivity of pure metals increases several orders of magnitude when they are cooled from room temperature to cryogenic temperatures. A commonly used parameter, the residual resistivity ratio (RRR), is defined (at 4 K) as $\mathrm{RRR} = \sigma_c(4\ \mathrm{K})/\sigma_c(293\ \mathrm{K})$. At the room temperature $|\zeta| \ll 1$ and the surface impedance reduces to the simple model of ac conductivity:

$$Z_s(k) = \sqrt{ikZ_0\frac{u}{\sigma_c}}. \tag{106}$$

Superconducting undulators (SCU) are part of the European XFEL facility development program [24]. A total of six SCU modules are planned to be installed downstream of the SASE2 undulator line at the European XFEL. The SCU vacuum chamber will have elliptical or racetrack shape with width $2w = 10$ mm and height $2a = 5$ mm. In the following we estimate the longitudinal wakefields of aluminum vacuum chamber at cryogenic temperature. The material properties of the aluminum at the room temperature are: $\sigma_c = 3.66\times10^7$ S/m, $\tau = 7.1\times10^{-15}$ s, $v_f = 2\times10^6$ m/s. At cryogenic temperature we assume that RRR = 100.

In the following we assume that the impedance matrix has only diagonal nonzero elements which are equal to $Z_s(k)$.

In Fig. 7 on the left we compare the longitudinal wake functions in the round chamber with radius of 2.5 mm. The blue dashed curve and the red dotted curve present the wake functions at the room temperature obtained with Eqs. (106) and (105), correspondingly. The solid black line presents the wake at the cryogenic temperature with RRR = 100. The wake functions of ac and ASE models at the room temperature are quite close and effect of ASE is small. All three wake functions have the same value at the origin given by $Z_0c/(\pi a^2)$. The wake at the cryogenic temperature drops faster but has a larger amplitude of oscillations.

The right plot in Fig. 7 presents dependence of the loss factor $\langle W_{||}\rangle$ from the rms bunch length σ_z for the Gaussian bunch shape. The loss factor is defined as

$$\langle W_{||}(s)\rangle = \int_{-\infty}^{\infty} W_{||}(s')\lambda(s')ds'. \tag{107}$$

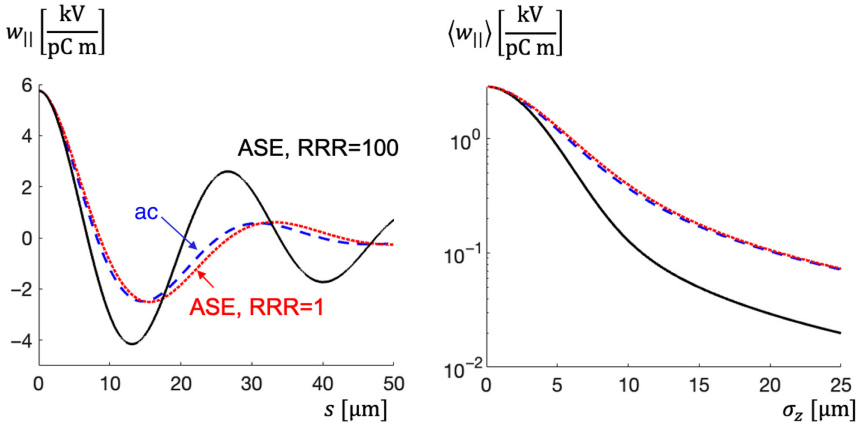

FIG. 7. The left plot shows the longitudinal wake functions of the round chamber with radius of 2.5 mm. The blue dashed curve and the red dotted curve present the wake functions at the room temperature obtained with Eqs. (106) and (105), correspondingly. The solid black line presents the wake at the cryogenic temperature with RRR = 100 The right plot presents dependence of the loss factor $\langle W_{||}\rangle$ form the rms bunch length σ_z for the Gaussian bunch shape for the three cases presented in the left plot.

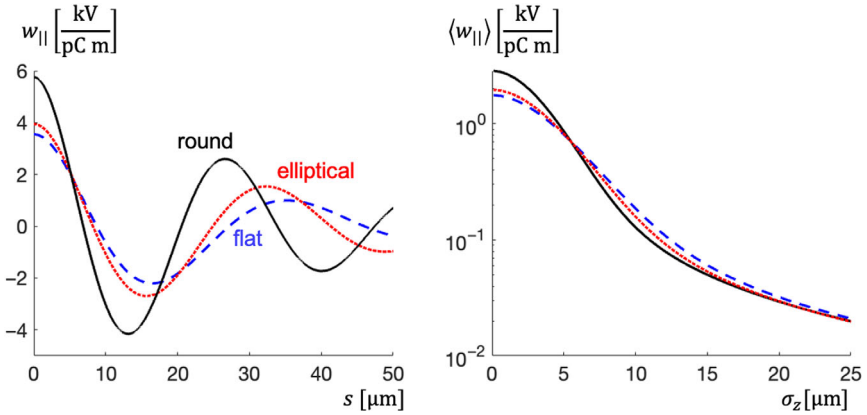

FIG. 8. The left plot compares the longitudinal wake functions of different vacuum chamber shapes at cryogenic temperature with RRR = 100. The right plot presents dependence of the loss factor $\langle W_{||}\rangle$ form the rms bunch length σ_z for the Gaussian bunch shape for the three cases presented in the left plot.

In Fig. 8 on the left we compare the longitudinal wake functions of different vacuum chamber shapes at cryogenic temperature with RRR = 100. The solid black line presents the wake of the round shape with radius a of 2.5 mm. The red dotted curve presents the wake of the elliptical shape with height $2a = 5$ mm and width $2w = 10$ mm. For the elliptical shape we have used the numerical code described in [25]. The red dotted curve presents the wake of two parallel plates with height $2a = 5$ mm. The reduction of the wake at the origin is equal to $\pi^2/16$ for the flat shape and $F^{\text{ellip}}(0.5) = 0.68$ for the elliptical one (see Appendix C for the definition of F^{ellip}). The right plot in Fig. 7 presents dependence of the loss factor $\langle W_{||}\rangle$ form the rms bunch length σ_z for the Gaussian bunch and the tree vacuum chamber cross sections. It is interesting to note that the other shapes reduce the loss factor (relative to the one of round pipe) only for very short bunches with rms length less than 6 μm.

The loss factor can be converted to the heating of the vacuum chamber walls: $P = f_{\text{rep}}\langle W_{||}\rangle Q^2$, where f_{rep} is the bunch repetition rate and Q is the bunch charge. Assuming $f_{\text{rep}} = 27$ kHz, $Q = 250$ pC and maximal peak current of 5 kA (which corresponds to $\sigma_z = 6$ μm) we obtain the same heat power $P = 1$ W/m for all three shapes of the vacuum chamber. The extra heating has to be taken into account in the design of the cryogenic system.

Finally as the last example we consider the impedance of the metallic pipe with dielectric coating which could be used for generation of terahertz radiation at the European XFEL. The application of two-layer metal-dielectric compounds as accelerating structure and as radiators for the generation of intense wakefield radiation are recognized as promising areas in which intensive theoretical and experimental research is being carried out.The fundamental importance of the finite conductivity

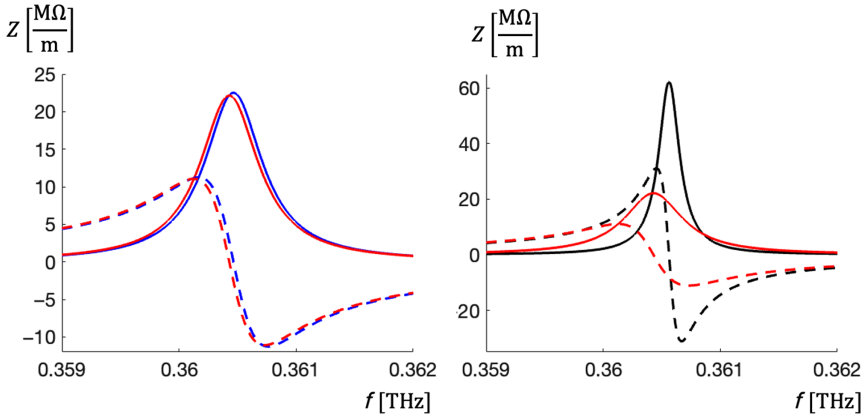

FIG. 9. The left plot compares the real (solid lines) and imaginary (dashed lines) parts of the longitudinal impedance of the round metallic pipe with dielectric layer at the room temperature near to the main resonance frequency. The blue lines are obtained with ac surface impedance, Eq. (106). The red lines are obtained with ASE surface impedance, Eq. (105). The right plot compares the impedances obtained with ASE surface impedance, Eq. (105), at the room temperate with RRR = 1 (red curves) and at the cryogenic temperature with RRR = 100 (black lines).

of the metallic wave-guide and of losses in the dielectric layer was underlined in [26].

We consider a cylindrical metal waveguide with an internal dielectric coating. The inner radius of the copper pipe with conductivity $\sigma_c = 5.8 \times 10^7$ S/m is $a = 0.55$ mm. The dielectric coating has thickness of 50 μm and permittivity $\epsilon = 9\epsilon_0$. The copper has the relaxation time $\tau = 2.46 \times 10^{-14}$ s and the Fermi velocity $v_f = 1.6 \times 10^6$ m/s. We assume that the dielectric is lossless and consider only losses in copper.

In Fig. 9 on the left we compare the real (solid lines) and imaginary (dashed lines) parts of the longitudinal impedance at the room temperature near to the main resonance frequency. The blue lines are obtained with ac surface impedance, Eq. (106). The red lines are obtained with ASE surface impedance, Eq. (105). The curves are quite similar.

The right plot in Fig. 9 compares the impedances obtained with ASE surface impedance, Eq. (105), at the room temperate (red curves) and at the cryogenic temperature (black curves). We have used RRR = 1 for the room temperature and RRR = 100 for the cryogenic one. As expected the cryogenic temperature allows to reduce the losses in the metal making only negligible shift in the resonance frequency.

V. DISCUSSION

We have thus far examined cases where the impedance matrix takes a uniform form across all modes within the modal expansion. This approach often yields a sufficiently accurate solution for various scenarios. However, a more refined approximation or even an exact problem reformulation can be achieved by introducing an impedance matrix that varies with the modal number m. For instance, consider the scenario of an infinitely thick cylindrical pipe with material parameters defined by Eq. (77). We can reformulate the problem as the solution of Maxwell's equations within the vacuum region, incorporating the impedance boundary condition, Eq. (5), where the impedance matrix is modally dependent with matrix elements

$$
\begin{aligned}
Z^m_{TM} &= -\frac{ia\nu^2 K_m(a\nu_\epsilon)}{ckm\epsilon_r K_m(a\nu_\epsilon) + ack\epsilon_r\nu_\epsilon K_{m-1}(a\nu_\epsilon)} \\
Z^m_{12} &= -\left(\frac{a\beta c\epsilon_r\nu_\epsilon K_{m-1}(a\nu_\epsilon)}{mK_m(a\nu_\epsilon)} + \beta c\epsilon_r\right)^{-1}, \\
Z^m_{21} &= -Z^m_{12}. \\
Z^m_{TE} &= \frac{1}{Z^m_{TM}}\left(\frac{\mu_r}{\epsilon_r} + Z^m_{12}Z^m_{21}\right) \\
&\quad - \frac{ick\mu_r}{\nu^2}\left(\frac{\nu_\epsilon K_{m-1}(a\nu_\epsilon)}{K_m(a\nu_\epsilon)} - \frac{\nu_\mu K_{m-1}(a\nu_\mu)}{K_m(a\nu_\mu)}\right).
\end{aligned}
$$

Here a is the interior radius of the pipe and other parameters are defined as in Eq. (78). For large conductivity, $\sigma_c \gg 1$, this matrix can be approximated by diagonal impedance matrix with elements given by Eq. (106). Similar modally dependent impedance matrix formulations are feasible for multilayered structures, as discussed in Ref. [16].

The equations derived in this paper remain valid even when considering an impedance matrix dependent on the modal number m.

In this study, we have exclusively presented corrugated structures as examples of surfaces with anisotropic impedance. Corrugated and dielectric waveguides are presently undergoing extensive investigation as accelerated structures or sources of terahertz radiation. Given that various materials (such as sapphire, ceramic films, etc.) exhibit significant anisotropy and that intentionally designed surfaces with desired anisotropy can be crafted as explored in Ref. [15], we anticipate that the findings from this work will offer valuable insights for designing different components of modern accelerators.

In the examples we have considered only the relativistic limit,$\gamma \to \infty$, without analysis of dependence of the results on the beam energy. For the round conductive pipe such kind of analysis for the monopole and dipole modes was carried out in [3].

VI. SUMMARY

In this paper, we have derived analytical expressions for beam impedance of round, rectangular and Π-shaped pipes with anisotropic surface impedance. We have considered both the relativistic and nonrelativistic cases. The field matching technique for layered structures with layers of uniaxial anisotropy and anisotropic impedance boundary condition at the last layer was described. The derived equations are applied to the case of corrugated structures with anisotropic impedance and closed analytical expressions for the wake functions with arbitrary offset of the source and the witness particles have been established. The influence of the shape of the vacuum chamber on the wakes in the cryogenic temperature was studied. It was shown that the shaping of the pipe allows to reduce the energy loss only for extremely short bunches. Finally the impact of the anomalous skin effect on the longitudinal impedance of metallic pipe with dielectric layer was analyzed.

APPENDIX A: MATRIX ELEMENTS FOR ROUND LAYERED WAVEGUIDE WITH UNIAXIAL ANISOTROPY

Here we consider the matrices used for many layered round pipe. The matrix $\mathbf{M}_j$ from Eq. (81) is a complex matrix of order 4 which maps coefficients from layer with index $j-1$ to the ones in layer j. In order to simplify the notation we use a for a_j, index "1" for $j-1$ and index "2" for j. Additionally we omit label r and use ν_ϵ, ν_μ instead of ν^ϵ_r, ν^μ_r. Then the matrix $\mathbf{M}_j$ has the following elements

$$M_{11} = \frac{1}{2}a\left(\frac{\nu_2^2\epsilon_{r,1}\nu_{\epsilon,1}[I_{m-1}(a\nu_{\epsilon,1}) + I_{m+1}(a\nu_{\epsilon,1})]K_m(a\nu_{\epsilon,2})}{\nu_1^2\epsilon_{r,2}} + \nu_{\epsilon,2}I_m(a\nu_{\epsilon,1})[K_{m-1}(a\nu_{\epsilon,2}) + K_{m+1}(a\nu_{\epsilon,2})]\right),$$
$$M_{12} = \frac{\nu_2^2\epsilon_{r,1}K_m(a\nu_{\epsilon,2})[mK_m(a\nu_{\epsilon,1}) - a\nu_{\epsilon,1}K_{m+1}(a\nu_{\epsilon,1})]}{\nu_1^2\epsilon_{r,2}} + K_m(a\nu_{\epsilon,1})[a\nu_{\epsilon,2}K_{m+1}(a\nu_{\epsilon,2}) - mK_m(a\nu_{\epsilon,2})]$$
$$M_{13} = \frac{\beta mc(\nu_2^2\mu_{r,1}\epsilon_{r,1} - \nu_1^2\mu_{r,2}\epsilon_{r,2})I_m(a\nu_{\mu,1})K_m(a\nu_{\epsilon,2})}{\nu_1^2\epsilon_{r,2}},$$
$$M_{14} = \frac{K_m(a\nu_{\mu,1})}{I_m(a\nu_{\mu,1})}M_{13},$$

$$M_{21} = \frac{1}{2}a\left(\nu_{\epsilon,2}I_m(a\nu_{\epsilon,1})[I_{m-1}(a\nu_{\epsilon,2}) + I_{m+1}(a\nu_{\epsilon,2})] - \frac{\nu_2^2\epsilon_{r,1}\nu_{\epsilon,1}I_m(a\nu_{\epsilon,2})[I_{m-1}(a\nu_{\epsilon,1}) + I_{m+1}(a\nu_{\epsilon,1})]}{\nu_1^2\epsilon_{r,2}}\right),$$
$$M_{22} = \frac{1}{2}a\left(\frac{\nu_2^2\epsilon_{r,1}\nu_{\epsilon,1}I_m(a\nu_{\epsilon,2})[K_{m-1}(a\nu_{\epsilon,1}) + K_{m+1}(a\nu_{\epsilon,1})]}{\nu_1^2\epsilon_{r,2}} + \nu_{\epsilon,2}[I_{m-1}(a\nu_{\epsilon,2}) + I_{m+1}(a\nu_{\epsilon,2})]K_m(a\nu_{\epsilon,1})\right)$$
$$M_{23} = \frac{\beta mc(\nu_1^2\mu_{r,2}\epsilon_{r,2} - \nu_2^2\mu_{r,1}\epsilon_{r,1})I_m(a\nu_{\mu,1})I_m(a\nu_{\epsilon,2})}{\nu_1^2\epsilon_{r,2}},$$
$$M_{24} = \frac{K_m(a\nu_{\mu,1})}{I_m(a\nu_{\mu,1})}M_{23},$$

$$M_{31} = \frac{c\beta m(\nu_2^2\mu_{r,1}\epsilon_{r,1} - \nu_1^2\mu_{r,2}\epsilon_{r,2})K_m(a\nu_{\mu,2})I_m(a\nu_{\epsilon,1})}{\nu_1^2\mu_{r,2}},$$
$$M_{32} = \frac{K_m(a\nu_{\epsilon,1})}{I_m(a\nu_{\epsilon,1})}M_{31},$$
$$M_{33} = \frac{1}{2}a\left(\nu_{\mu,2}I_m(a\nu_{\mu,1})[K_{m-1}(a\nu_{\mu,2}) + K_{m+1}(a\nu_{\mu,2})] + \frac{\nu_2^2\nu_{\mu,1}\mu_{r,1}[I_{m-1}(a\nu_{\mu,1}) + I_{m+1}(a\nu_{\mu,1})]K_m(a\nu_{\mu,2})}{\nu_1^2\mu_{r,2}}\right)$$
$$M_{34} = K_m(a\nu_{\mu,1})[a\nu_{\mu,2}K_{m+1}(a\nu_{\mu,2}) - mK_m(a\nu_{\mu,2})] + \frac{\nu_2^2\mu_{r,1}K_m(a\nu_{\mu,2})[mK_m(a\nu_{\mu,1}) - a\nu_{\mu,1}K_{m+1}(a\nu_{\mu,1})]}{\nu_1^2\mu_{r,2}},$$

$$M_{41} = \frac{c\beta m(\nu_1^2\mu_{r,2}\epsilon_{r,2} - \nu_2^2\mu_{r,1}\epsilon_{r,1})I_m(a\nu_{\mu,2})I_m(a\nu_{\epsilon,1})}{\nu_1^2\mu_{r,2}},$$
$$M_{42} = \frac{K_m(a\nu_{\epsilon,1})}{I_m(a\nu_{\epsilon,1})}M_{41},$$
$$M_{43} = \frac{1}{2}a\left(\nu_{\mu,2}I_m(a\nu_{\mu,1})[I_{m-1}(a\nu_{\mu,2}) + I_{m+1}(a\nu_{\mu,2})] - \frac{\nu_2^2\nu_{\mu,1}\mu_{r,1}I_m(a\nu_{\mu,2})[I_{m-1}(a\nu_{\mu,1}) + I_{m+1}(a\nu_{\mu,1})]}{\nu_1^2\mu_{r,2}}\right),$$
$$M_{44} = \frac{1}{2}a\left(\nu_{\mu,2}[I_{m-1}(a\nu_{\mu,2}) + I_{m+1}(a\nu_{\mu,2})]K_m(a\nu_{\mu,1}) + \frac{\nu_2^2\nu_{\mu,1}\mu_{r,1}I_m(a\nu_{\mu,2})[K_{m-1}(a\nu_{\mu,1}) + K_{m+1}(a\nu_{\mu,1})]}{\nu_1^2\mu_{r,2}}\right).$$

Matrix $\mathbf{M}_N^{C2F}$ converts the field coefficients into the field components and its nonzero elements are

$$M_{11}^{C2F} = I_m(a_N\nu_{\epsilon,N}), \qquad M_{12}^{C2F} = K_m(a_N\nu_{\epsilon,N}),$$
$$M_{23}^{C2F} = I_m(a_N\nu_{\mu,N}), \qquad M_{24}^{C2F} = K_m(a_N\nu_{\mu,N}),$$

$$M_{31}^{C2F} = -\frac{ikmI_m(a_N\nu_{\epsilon,N})}{\beta a_N\nu_N^2},$$
$$M_{32}^{C2F} = -\frac{ikmK_m(a_N\nu_{\epsilon,N})}{\beta a_N\nu_N^2},$$
$$M_{33}^{C2F} = -\frac{ikc\nu_{\mu,N}\mu_{r,N}[I_{m-1}(a_N\nu_{\mu,N}) + I_{m+1}(a_N\nu_{\mu,N})]}{2\nu_N^2},$$
$$M_{34}^{C2F} = \frac{ikc\nu_{\mu,N}\mu_{r,N}[K_{m-1}(a_N\nu_{\mu,N}) + K_{m+1}(a_N\nu_{\mu,N})]}{2\nu_N^2},$$

$$M_{41}^{C2F} = \frac{ikc\epsilon_{r,N}\nu_{\epsilon,N}[I_{m-1}(a_N\nu_{\epsilon,N}) + I_{m+1}(a_N\nu_{\epsilon,N})]}{2\nu_N^2},$$
$$M_{42}^{C2F} = -\frac{ikc\epsilon_{r,N}\nu_{\epsilon,N}[K_{m-1}(a_N\nu_{\epsilon,N}) + K_{m+1}(a_N\nu_{\epsilon,N})]}{2\nu_N^2},$$
$$M_{43}^{C2F} = \frac{ikmI_m(a_N\nu_{\mu,N})}{\beta a_N\nu_N^2},$$
$$M_{44}^{C2F} = \frac{ikmK_m(a_N\nu_{\mu,N})}{\beta a_N\nu_N^2}.$$

APPENDIX B: MATRIX ELEMENTS FOR RECTANGULAR AND Π-SHAPED ANISOTROPIC LAYERED WAVEGUIDES

In the case of rectangular structure with many layers matrix $\mathbf{M}_j$ relates coefficients at interface $r = a_j$

$$\left(C_+^{m,j}, C_-^{m,j}, D_+^{m,j}, D_-^{m,j}\right)^T = \mathbf{M}_j\left(C_+^{m,j-1}, C_-^{m,j-1}, D_+^{m,j-1}, D_-^{m,j-1}\right)^T.$$

In order to simplify the notation we use a for a_j, index "1" for $j-1$ and index "2" for j. Additionally we omit label y and use k_ϵ, k_μ instead of k_y^ϵ, k_y^μ.

The matrix $\mathbf{M}_j$ has the following elements

$$M_{11} = \frac{e^{a(k_{\epsilon,1}-k_{\epsilon,2})}(\nu_1^2 k_{\epsilon,2}\epsilon_{y,2} + \nu_2^2 k_{\epsilon,1}\epsilon_{y,1})}{2\nu_1^2 k_{\epsilon,2}\epsilon_{y,2}},$$
$$M_{12} = \frac{e^{-a(k_{\epsilon,1}+k_{\epsilon,2})}(\nu_1^2 k_{\epsilon,2}\epsilon_{y,2} - \nu_2^2 k_{\epsilon,1}\epsilon_{y,1})}{2\nu_1^2 k_{\epsilon,2}\epsilon_{y,2}},$$
$$M_{13} = \frac{\beta c k_x e^{a(k_{\mu,1}-k_{\epsilon,2})}(\nu_1^2\mu_{y,2}\epsilon_{y,2} - \nu_2^2\mu_{y,1}\epsilon_{y,1})}{2\nu_1^2 k_{\epsilon,2}\epsilon_{y,2}},$$
$$M_{14} = e^{-2ak_{\mu,1}}M_{13},$$
$$M_{21} = e^{2a(k_{\epsilon,1}+k_{\epsilon,2})}M_{12}, \qquad M_{22} = e^{2a(k_{\epsilon,2}-k_{\epsilon,1})}M_{11},$$
$$M_{23} = -e^{2ak_{\epsilon,2}}M_{13}, \qquad M_{24} = -e^{2a(k_{\epsilon,2}-k_{\mu,1})}M_{13},$$
$$M_{31} = -e^{2a(k_{\epsilon,1}-k_{\mu,2})}M_{42}, \qquad M_{32} = -e^{-2ak_{\mu,2}}M_{42},$$
$$M_{33} = e^{2a(k_{\mu,1}-k_{\mu,2})}M_{44}, \qquad M_{34} = e^{-2a(k_{\mu,1}+k_{\mu,2})}M_{43},$$
$$M_{41} = e^{2ak_{\epsilon,1}}M_{42},$$
$$M_{42} = \frac{c\beta k_x e^{a(k_{\mu,2}-k_{\epsilon,1})}(\nu_2^2\mu_{y,1}\epsilon_{y,1} - \nu_1^2\mu_{y,2}\epsilon_{y,2})}{2\nu_1^2 k_{\mu,2}\mu_{y,2}},$$
$$M_{43} = \frac{e^{a(k_{\mu,1}+k_{\mu,2})}(\nu_1^2 k_{\mu,2}\mu_{y,2} - \nu_2^2 k_{\mu,1}\mu_{y,1})}{2\nu_1^2 k_{\mu,2}\mu_{y,2}},$$
$$M_{44} = \frac{e^{a(k_{\mu,2}-k_{\mu,1})}(\nu_1^2 k_{\mu,2}\mu_{y,2} + \nu_2^2 k_{\mu,1}\mu_{y,1})}{2\nu_1^2 k_{\mu,2}\mu_{y,2}}.$$

The matrix $\mathbf{M}_N^{C2F}$ converts the field coefficients into the field components:

$$(E_{z,m}(a_N), H_{z,m}(a_N), E_{x,m}(a_N), H_{x,m}(a_N))^T = \mathbf{M}_N^{C2F}(C_+^{m,N}, C_-^{m,N}, D_+^{m,N}, D_-^{m,N})^T.$$

The nonzero elements of this matrix are

$$M_{11}^{C2F} = e^{a_N k_{\epsilon,N}}, \quad M_{12}^{C2F} = e^{-a_N k_{\epsilon,N}},$$
$$M_{23}^{C2F} = e^{a_N k_{\mu,N}}, \quad M_{24}^{C2F} = e^{-a_N k_{\mu,N}},$$
$$M_{31}^{C2F} = \frac{ikk_x e^{a_N k_{\epsilon,N}}}{\beta\nu_N^2}, \quad M_{32}^{C2F} = \frac{ikk_x e^{-a_N k_{\epsilon,N}}}{\beta\nu_N^2},$$
$$M_{33}^{C2F} = -\frac{ikZ_0 k_{\mu,N}\mu_{y,2N}e^{a_N k_{\mu,N}}}{\nu_N^2},$$
$$M_{34}^{C2F} = \frac{ikZ_0 k_{\mu,N}\mu_{y,2N}e^{-a_N k_{\mu,N}}}{\nu_N^2},$$
$$M_{41}^{C2F} = \frac{ickk_{\epsilon,N}\epsilon_{y,N}e^{a_N k_{\epsilon,N}}}{\nu_N^2}, \quad M_{42}^{C2F} = -\frac{ickk_{\epsilon,N}\epsilon_{y,N}e^{-a_N k_{\epsilon,N}}}{\nu_N^2},$$
$$M_{43}^{C2F} = -\frac{ikk_x e^{a_N k_{\mu,N}}}{\beta\nu_N^2}, \quad M_{44}^{C2F} = -\frac{ikk_x e^{-a_N k_{\mu,N}}}{\beta\nu_N^2}.$$

APPENDIX C: SHORT-RANGE LONGITUDINAL FORM FACTORS OF ELLIPTICAL AND RECTANGULAR WAVEGUIDES

It is well known that the longitudinal wake function of round pipe of radius a with a retardation layer has the following value at the origin

$$w_\parallel^{\text{round}}(0) = \frac{Z_0 c}{2\pi a^2}, \qquad w_\parallel^{\text{round}}(0+) = 2w_\parallel^{\text{round}}(0),$$

where "0+" means the one-sided limit from the right.

An ellipse with semimajor axis w and semiminor axis a can be conformally mapped onto the circle of radius a by transformation

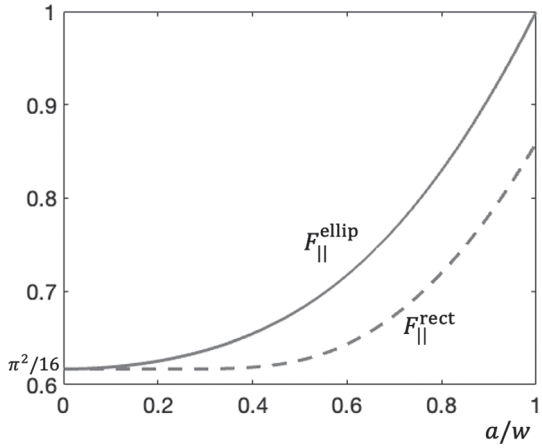

FIG. 10. Short-range longitudinal form factors of the elliptical (solid line) and the rectangular (dashed line) pipes.

$$f^{\mathrm{ellip}}(z) = a\sqrt{k}\,\mathrm{sn}\left(\frac{2K}{\pi}\arcsin\left(\frac{z}{\sqrt{(w^2-a^2)}}\right), k^2\right),$$

where sn is the Jacobi elliptic sine function and

$$k = \left(\frac{\theta_2(0,p)}{\theta_3(0,p)}\right)^2, \quad K = \frac{\pi}{2}\theta_3^2(0,p), \quad p = \left(\frac{w-a}{w+a}\right)^2.$$

Here θ_2, θ_3 are Jacobi theta functions. Following [27] we can write the value of the longitudinal wake function of the elliptical wave-guide at the origin as

$$w_{\|}^{\mathrm{ellip}}(0) = w_{\|}^{\mathrm{round}}(0)F_{\|}^{\mathrm{ellip}}\left(\frac{a}{w}\right),$$
$$F_{\|}^{\mathrm{ellip}}\left(\frac{a}{w}\right) = \left(\frac{d}{dz}f^{\mathrm{ellip}}[0]\right)^2 = \left(\frac{a}{w}\right)^2\frac{4kK^2}{\pi^2[1-(a/w)^2]},$$

where $F_{\|}^{\mathrm{ellip}}$ is the longitudinal form factor of the elliptical wave-guide.

A rectangle with width $2w$ and height $2a$ can be conformally mapped onto the circle of radius g by transformation

$$f^{rect}(z) = g\frac{1+i\sqrt{k}\,\mathrm{sn}[Kw^{-1}(z+ia)]}{i+\sqrt{k}\,\mathrm{sn}[Kw^{-1}(z+ia)]},$$

where the symbols K and k have the same meaning as for the ellipse above but the value of p is different:

$$p = e^{-2\pi a/w}.$$

Hence the longitudinal wake function of the rectangular waveguide at the origin can be written as

$$w_{\|}^{\mathrm{rect}}(0) = w_{\|}^{\mathrm{round}}(0)F_{\|}^{\mathrm{rect}}\left(\frac{a}{w}\right),$$
$$F_{\|}^{\mathrm{rect}}\left(\frac{a}{w}\right) = \left(\frac{d}{dz}f^{\mathrm{rect}}[0]\right)^2 = \left(\frac{a}{w}\right)^2\frac{4kK^2(\mathrm{cn}(iK\frac{a}{w},k^2)\,\mathrm{dn}(iK\frac{a}{w},k^2))^2}{(i+\sqrt{k}\,\mathrm{sn}(iK\frac{a}{w},k^2))^4},$$

where sn, cn, dn are elliptic Jacobi functions and $F_{\|}^{\mathrm{rect}}$ is the longitudinal form factor of the rectangular waveguide.

The form factors allow simple cubic approximations:

$$F_{\|}^{\mathrm{ellip}}(x) = 0.279x^3 + 0.093x^2 + 0.013x + \pi^2/16,$$
$$F_{\|}^{\mathrm{rect}}(x) = 0.477x^3 - 0.268x^2 + 0.036x + \pi^2/16,$$
$$x = a/w, \qquad a \le w,$$

with maximal absolute error below 0.3%. Figure 10 shows dependence of the form factors from the parameters ratio a/w.

[1] J. D. Jackson, *Classical Electrodynamics* (John Wiley & Sons, New York, 1999), 3rd ed..

[2] M. Dohlus, Impedance of beam pipes with smooth shallow corrugations, DESY TESLA Report No. 2001-26, 2001.

[3] G. Stupakov, Resistive-wall wake for non-relativistic beam revisited, Phys. Rev. Accel. Beams **23**, 094401 (2020).

[4] K. Bane and G. Stupakov, Roughness tolerance studies for the undulator beam pipe chamber of LCLS-II, *27th Linear Accelerator Conference, Geneva, Switzerland, 2014* (CERN, Geneva, 2014); Report No. LCLS-II-TN-14-06, 2014.

[5] G. Stupakov and K. L. F. Bane, Surface impedance formalism for a metallic beam pipe with small corrugations, Phys. Rev. ST Accel. Beams **15**, 124401 (2012).

[6] K. Bane and G. Stupakov, Dechirper wakefields for short bunches, Nucl. Instrum. Methods Phys. Res., Sect. A **820**, 156 (2016).

[7] K. Bane, G. Stupakov, and I. Zagorodnov, Analytical formulas for short bunch wakes in a flat dechirper, Phys. Rev. Accel. Beams **19**, 084401 (2016).

[8] K. Bane, G. Stupakov, and I. Zagorodnov, Wakefields of a Beam near a Single Plate in a Flat Dechirper, SLAC National Accelerator Laboratory Technical Report No. SLAC-PUB-16881, 2016.

[9] G. Stupakov, K. L. F. Bane, P. Emma, and B. Podobedov, Resistive wall wakefields of short bunches at cryogenic temperatures, Phys. Rev. ST Accel. Beams **18**, 034402 (2015).

[10] G. E. H. Reuter and E. H. Sondheimer, The theory of the anomalous skin effect in metals, Proc. R. Soc. A **195**, 336 (1948).

[11] B. W. Zotter and S. A. Kheifets, *Impedances and Wakes in High-Energy Particle Accelerators* (World Scientific, Singapore, 1998).

[12] K. Bane, G. Stupakov, and E. Gjonaj, Joule heating in a flat dechirper, Phys. Rev. Accel. Beams **20**, 054403 (2017).
[13] E. S. Simakov, A. V. Tyukhtin, and S. N. Galyamin, Radiation of a charge moving along a corrugated surface with a relatively small period, Phys. Rev. Accel. Beams **22**, 061301 (2019).
[14] E. S. Simakov and A. V. Tyukhtin, Radiation of a charged particle bunch moving along a deeply corrugated structure with a relatively small period, Nucl. Instrum. Methods Phys. Res., Sect. A **1028**, 166387 (2022).
[15] R. Quarfoth, Anisotropic artificial impedance surfaces, PhD thesis, UC, San Diego, 2014.
[16] D. J. Hoppe and Y. Rahmat-Samii, *Impedance Boundary Conditions in Electromagnetics* (CRC Press, Boca Raton, 1995).
[17] S. V. Yuferev and N. Ida, *Surface Impedance Boundary Conditions: A comprehensive Approach* (CRC Press, Boca Raton, 2010).
[18] N. Mounet, The LHC Transverse Coupled-Bunch Instability, Ph.D. thesis, EPFL, Lausanne, 2012.
[19] I. Zagorodnov, Impedances of anisotropic round and rectangular chambers, Phys. Rev. Accel. Beams **21**, 064601 (2018).
[20] Wolfram Research, Inc., Mathematica, Version 13.3, Champaign, IL (2023).
[21] I. Zagorodnov, K. L. F. Bane, and G. Stupakov, Calculation of wakefields in 2D rectangular structures, Phys. Rev. ST Accel. Beams **18**, 104401 (2015).
[22] K. Yokoya and K. Bane, The longitudinal high-frequency impedance of a periodic accelerating structure, in *Proceedings of the 1999 Particle Accelerator Conference* (IEEE, Piscataway, 1999) p. 1725.
[23] W. Qin, M. Dohlus, and I. Zagorodnov, Short-range wakefields in an L-shaped corrugated structure, Phys. Rev. Accel. Beams **26**, 064402 (2023).
[24] S. Casalbuoni *et al.*, Superconducting undulator activities at the European X-ray Free-Electron Laser Facility, Front. Phys. **11**, 1204073 (2023).
[25] I. Zagorodnov, M. Dohlus, and T. Wohlenberg, Short-range longitudinal wake function of undulator lines at the European X-Ray Free Electron Laser, Nucl. Instrum. Methods Phys. Res., Sect. A **1043**, 167490 (2022).
[26] M. I. Ivanyan, L. V. Aslyan, K. Floettmann, and F. Lemery, Transverse impedance of lossy circular metal-dielectric structures, in *Proceedings of International Particle Accelerator Conference, IPAC-2021, SP, Brazil* (JACoW, Geneva, Switzerland, 2021), TUPAB269.
[27] S. S. Baturin and A. D. Kanareykin, New method of calculating the wakefields of a point charge in a waveguide of arbitrary cross section, Phys. Rev. Accel. Beams **19**, 051001 (2016).